Gallbladder cancer-associated fibroblasts promote vasculogenic mimicry formation and tumor growth of gallbladder cancers via upregulating the expression of NOX4, a poor prognosis factor, through activating IL-6-JAK-STAT3 signal pathway

Musu Pan
Tongji University https://orcid.org/0000-0002-0068-5383
Hui Wang
Tongji University
Kamar Hasan Ansari
Tongji University
Xin-Ping Li
Tongji University
Wei Sun
Tongji University
Yue-Zu Fan (fanyuezu@hotmail.com)
Tongji University

Research

Keywords: Gallbladder neoplasm, Gallbladder cancer-associated fibroblasts, Vasculogenic mimicry, NOX4, Signaling pathway, Prognosis

Posted Date: August 26th, 2020

DOI: https://doi.org/10.21203/rs.3.rs-64358/v1

Version of Record: A version of this preprint was published on November 5th, 2020. See the published version at https://doi.org/10.1186/s13046-020-01742-4.

Abstract

Background Cancer-associated fibroblasts (CAFs) and vasculogenic mimicry (VM) play important roles in the occurrence and development of tumors. However, the relationship between CAFs and VM formation, especially in gallbladder cancer (GBC) has not been clarified. In this study, we investigated whether gallbladder CAFs (GCAFs) can promote VM formation and tumor growth and explored the underlying molecular mechanism.

Methods A co-culture system of human GBC cells and fibroblasts or HUVECs was established. VM formation, proliferation, invasion, migration, tube formation assays, CD_{31}-PAS double staining, optic/electron microscopy and tumor xenograft assay were used to detect VM formation and malignant phenotypes of 3-D co-culture matrices *in vitro*, as well as the VM formation and tumor growth of xenografts *in vivo*, respectively. Microarray analysis was used to analyze gene expression profile in GCAFs/NFs and VM (+)/VM (-) *in vitro*. QRT-PCR, western blotting, IHC and CIF were used to detected NOX4 expression in GCAFs/NFs, 3-D culture/co-culture matrices *in vitro*, the xenografts *in vivo* and human gallbladder tissue/stroma samples. The correlation between NOX4 expression and clinicopathological and prognostic factors of GBC patients was analyzed. And, the underlying molecular mechanism of GCAFs promoting VM formation and tumor growth in GBC was explored.

Results GCAFs promote VM formation and tumor growth in GBC; and the finding was confirmed by facts that GCAFs induced proliferation, invasion, migration and tube formation of GBC cells *in vitro*, and promoted VM formation and tumor growth of xenografts *in vivo*. NOX4 is highly expressed in GBC and its stroma, which is the key gene for VM formation, and is correlated with tumor aggression and survival of GBC patients. The GBC patients with high NOX4 expression in tumor cells and stroma have a poor prognosis. The underlying molecular mechanism may be related to the up-regulation of NOX4 expression through paracrine IL-6 mediated IL-6/JAK/STAT3 signaling pathway.

Conclusions GCAFs promote VM formation and tumor growth in GBC *via* upregulating NOX4 expression through the activation of IL-6-JAK-STAT3 signal pathway. NOX4, as a VM-related gene in GBC, is over-expressed in GBC cells and GCAFs, which is related to aggression and unfavorable prognosis of GBC patients.

Introduction

Gallbladder cancer (GBC) is a highly malignant primary tumor of the biliary tract. Due to the lack of specific clinical manifestations and effective monitoring indicators, the early diagnosis rate of GBC is low. At the same time, the disease also has the characteristics of high invasion and metastasis, insensitivity to chemo-radiotherapy, resulting in disappointing surgical and drug treatment results and poor prognosis; according to relevant reports, its 5-year survival rate is only about 5% [1–3]. Therefore, it is of great significance to understand the pathogenesis of GBCs and explore the effective prognosis indicators and drug targets, so as to improve the diagnosis, treatment and prognosis of GBC patients.

It is generally believed that the occurrence and development of tumor is not only related to tumor itself, but also depends on the complex interaction between malignant cells and their microenvironment. Tumor microenvironment (TME), also known as tumor stroma, is composed of extracellular matrix (ECM) and a variety of stromal cells [4–5]. Cancer-associated fibroblasts (CAFs) are the most important stromal cells in TME, which play an important role in tumor growth and development, and participate in many biological processes such as tumor proliferation, invasion and metastasis, angiogenesis [6–10], and are related to poor prognosis [11]. In these biological processes, angiogenesis and effective blood supply are the basic conditions for tumor growth and metastasis [12]. In recent years, studies have found a novel tumor blood supply pattern, called vasculogenic mimicry (VM), which occurs in certain highly aggressive malignancies, and is closely related to poor clinical results and poor prognosis [13–16]. It has become one of the potential targets for anticancer therapy [17–20]. We previously reported that VM exists in GBC and is associated with the patient's poor prognosis. The mechanism of VM formation in GBC may be closely related to the activation of PI3K/MMPs/Ln-5γ2 and/or EphA2/FAK/Paxillin signaling pathways [14–19]. Recently, it was reported that CAFs can promote VM formation in hepatocellular cancer (HCC) [21]. However, so far, the mechanism of VM formation is not clear, and the relationship between gallbladder cancer-associated fibroblasts (GCAFs) and VM formation in GBC has not been reported.

NOX4 (nicotinamide adenine dinucleotide phosphate oxidase 4, NADPH oxidase 4) is a number of NADPH oxidase (NOX) family [22, 23]. NOX family plays vital roles in signaling transduction, cell growth, apoptosis, differentiation and tumor development. Long-term oxidation/reduction imbalance is considered to be one of the important factors leading to carcinogenesis. Oxidative stress induces the development of cancer due to excessive production of reactive oxygen species (ROS) by members of the NOX family [24–27]. It was reported that NOX4 is overexpressed in many malignancies and participates in malignant processes such as proliferation and metastasis [22, 28]; NOX4 can also promote tumor angiogenesis by regulating the production of vascular endothelial growth factor, which further results in poor prognosis [29].

In this study, we firstly found that GCAFs can promote VM formation and tumor growth of GBC; NOX4, as a key gene of VM formation in GBC, is over-expressed in GBC and its stroma, which is related to poor prognosis. At the same time. We also proved that GCAFs promote VM formation and tumor growth of GBCs via upregulating NOX4 expression through paracrine IL-6 mediated IL-6-JAK-STAT3 signal pathway.

Materials And Methods

Cell lines and cultures

Three established human GBC cell lines, GBC-SD (Shanghai Cell Biology Research Institute of Chinese Academy of Sciences, CAS, China), SGC-996 (Gift from Professor Yao-Qin Yang, Institute of tumor cytology, Medical College of Tongji University), OCUG-1 (Gift from Professor Liu YB, Professor Ying-Bin Liu, Shanghai Xinhua Hospital), and TJ-GBC2 (A novel GBC cell line, constructed in our laboratory [30]) were used in this study. These cells were propagated in Dulbecco's modified Eadles medium (DMEM,

Gibco, USA) supplemented with 10% fetal bovine serum (FBS, Ausbian, Australia) and 0.1% gentamicin sulfate (Gemini Bioproducts, Calabasas, Calif). The established human umbilical vein endothelial cell line (HUVEC, gift from Department of Pathophysiology, Shanghai Medical College, Fudan University) was cultured in endothelial cell medium (ECM, Sciencell, USA) with 10% FBS. Human GCAFs and normal fibroblasts (NFs) were isolated from the clinical specimens of human GBC tissues and adjacent normal tissues, and identified by the detection of the stromal markers α-smooth muscle actin (α-SMA) and fibroblast activation protein (FAP) using immunohistochemistry (IHC), co-immunofluorescence (CIF) and western blotting. The established GCAFs and NFs (the cells used in this experiment were between the 4th and 9th generation) were incubated in DMEM/F-12 medium (Gibco; USA) supplemented with 10% FBS. Co-cultures of GBC cells and GCAFs or NFs were performed as previously described [11]. All of the cells were maintained in a carbon dioxide (CO_2) incubator (SANYO MCO-175, Japan) at 37˚C with a 5% CO_2 atmosphere.

VM formation assay in vitro

The Transwell chamber (aperture 0.4 μm, diameter 6.5 mm) was used to establish a co-culture system of human GBC cells and fibroblasts. Human GBC cell lines (GBC-SD, SGC-996 and OCUG-1) and fibroblasts (GCAFs or NFs) were used to prepare cell suspensions (GBC cells, $4 \times 10^4 \cdot ml^{-1}$; fibroblasts, $2 \times 10^4 \cdot ml^{-1}$). Matrigel and rat-tail type I collagen three-dimensional (3-D) matrices (ABI, USA) were prepared as described previously [15], coated on the bottom of the lower chamber respectively for comparative test. Cells were divided into GBC cell (GBC-SD), GBC cell (GBC-SD) + NFs and GBC cell (GBC-SD) + GCAFs groups. In the analysis of VM related gene expression profile, cells were divided into GBC cell (GBC-SD, SGC-996 or OCUG-1) group and GBC cell (GBC-SD, SGC-996 or OCUG-1) + GCAFs co-culture group. 50 μl GBC cell suspensions (5 × 104·ml-1) were injected into the lower chamber containing different gels separately and incubated for 2 h, then DMEM/F12 medium containing 100 $U \cdot ml^{-1}$ penicillin and streptomycin (containing 0.2% FBS) was added. The same amount of (200 μl) fibroblast suspensions (2×10^4/ml) or serum-free medium were added to the upper chamber. The culture medium was changed every 2–3 days. The formation of VM in 3-D matrices from GBC cells or co-cultures was performed by hematoxylin and eosin (H&E) staining and immunohistochemical periodic acid-Schiff (PAS) staining (without hematoxylin counterstain) as described previously [15, 18, 19], and was observed under an inverted optical microscope (Caikang XDS-100) every day, and the number of VM formation was recorded in 5 visual fields at 200 magnifications.

Assays of malignant phenotypes of GBCs triggered GCAFs in vitro

To verify that GCAFs promoted VM formation of GBCs, in following experiments we detected malignant phenotypes including proliferation, invasion, migration and tube formation of GBC cells triggered by GCAFs *in vitro*.

Cell proliferation was assessed using CCK-8 method. Cells were divided into GBC cell (GBC-SD, SGC-996 or TJ-GBC2) group, GBC cell (GBC-SD, SGC-996 or TJ-GBC2) + NFs co-culture group and GBC cell (GBC-SD,

SGC-996 or TJ-GBC2) + GCAFs co-culture group. A co-culture model of GBC cells and fibroblasts (GCAFs or NFs) was established by Transwell chamber (Corning, USA) with aperture of 0.4 μm and diameter of 6.5 mm. Lower chambers were inoculated with 700 μl GBC cell suspensions (4×10^4/ml), upper chambers inoculated with 200 μl GCAFs suspensions ($2 \times 10^4 \cdot ml^{-1}$) or equal volume serum-free medium. After 24 h, 36 h and 48 h of culture, CCK-8 solution (10 μl/well) was added, and the culture was continued for 1 h. The optical density (OD) value of each well was measured by enzyme-labeled instrument (Elx800UV, BIO-TEK, USA) at 450 nm wavelength. All experiments were performed in triplicate.

Cell invasion was assessed using the Transwell chambers with aperture of 8 μm and diameter 6.5 mm (Corning, USA). Matrigel (200 μl/well, BD, USA) was coated on the bottom of the upper chamber to simulate the basement membrane and extracellular matrix. Cells were grouped as above. GBC-SD, SGC-996 and TJ-GBC2 cell suspensions ($1 \times 10^5 \cdot ml^{-1}$; 200 μl) were respectively inoculated on the gel in the upper chambers. Lower chambers were inoculated with 700 μl NFs, GCAFs ($5 \times 10^4 \cdot ml^{-1}$) or serum-free medium. After 24 h of culture, the cells invaded through the basement membrane were stained with Giemsa (Beyotime, China) and counted under an inverted optical microscope (Caikang XDS-100, Shanghai, China). All experiments were performed in triplicate.

Cell migration was assessed with a wound healing assay. Cells were grouped as above. 100 μl GBC cell suspensions (5×10^4 cells/well) or equal volume co-culture cells (50 μl GBC cell suspensions, 50 μl NFs or GCAFs; $5 \times 10^4 \cdot ml^{-1}$) containing NFs, GCAFs or serum-free medium were inoculated into 96-well wounding plate (Coster, USA) with culture medium and cultured in a single layer for 24 h until 90% cells fused. Then, a scratch tester was used to scratch a wound at the central bottom of 96-well plate. Cell migration areas were scanned and analyzed at 0 h, 8 h and 24 h using a Cellomocs (Thermo Fisher Scientific, USA), and observed under an inverted optical microscope (Caikang XDS-100) at 200 magnifications. Cell migration area (pixel area) = (S3 + S4) - (S1 + S2). All experiments were performed in triplicate.

Tube formation was assessed with the model of interaction between GBC cells, GCAFs, NFs and HUVECs established by using Transwell chamber (aperture 0.4 μm, diameter 6.5 mm). The bottom of 24-well plate was covered with Matrigel (200 μl/well) to provide 3-D growth space for HUVECs. Cell suspensions (HUVEC $1 \times 10^4 \cdot ml^{-1}$; NFs or GCAFs $3 \times 10^4 \cdot ml^{-1}$; GBC-SD $2 \times 10^4 \cdot ml^{-1}$) were made by adding serum-free DMEM/F12 or ECM (HUVEC only). Cells were divided into HUVECs, HUVECs + GBC-SD, HUVECs + GBC-SD + NFs and HUVECs + GBC-SD + GCAFs groups, i.e. lower chambers were inoculated with 200 μl HUVECs; the upper chamber was respectively added with 200 μl serum-free medium, GBC-SD cell suspensions, GBC-SD + NFs cell suspensions or GBC-SD + GCAFs cell suspensions. During 48 h of cell culture, the lumen formation was observed dynamically under an inverted optical microscope (Caikang XDS-100), and the number of the lumen formed by HUVECs was counted. All experiments were performed in triplicate.

Tumor Xenograft assay in vivo

The xenograft experiments were performed in accordance with the official recommendations of Chinese Community Guidelines, and were approval from Research Ethical Review Broad in Tongji University (Shanghai, China). BALB/C nu/nu mice (equal numbers of male and female mice, 4-week old, about 20 g) were purchased from Shanghai Laboratory Animal Center, Chinese Academy of Sciences, and housed under specific pathogen-free (SPF) conditions. The mice were randomly divided into GBC-SD group and GBC-SD + GCAFs group, 10 mice in each group. 0.2 ml serum-free medium containing GBC-SD or GBC-SD + GCAFs co-culture cell suspensions ($5.0 \times 10^6 \cdot ml^{-1}$) were respectively injected subcutaneously into the right axilback of the nude mice. Tumor xenograft size i.e. the maximum diameter (a) and minimum diameter (b) was measured with calipers twice a week. The tumor volume was calculated by the following formula: V (cm^3) = Пab2/6. After 7 weeks, mice were sacrificed and xenograft specimens were used for western blotting, or were paraffin-embedded, deparaffinized, hydrated and were then used for immunohistochemistry (IHC) staining and Co-immunofluorescence (CIF) staining, respectively.

VM formation assay of tumor xenografts in vivo

VM formation assay of xenograft sections *in vivo* was conducted by H&E staining, CD31-PAS double staining and transmission electron microscopy (TEM) as described previously [15, 18, 19]. Histomorphologic appearance and VM characteristic of the tumor xenografts *in vivo* were observed under an inverted optical microscope (Caikang XDS-100) and a JEOL-1230 TEM (Japanese Electronics, Japan).

Patients and clinical specimens

From 2007 to 2011, 85 patients with GBC, 10 patients with gallbladder precancerous lesion or benign lesion were recruited from Tongji Hospital, Tongji University (Shanghai, China). This study was conducted in accordance with the official recommendations of ethical standards, the Declaration of Helsinki and the Chinese Community Guidelines, and was approved by the Ethics Committee and the Institutional Review Board of Tongji Hospital. A written informed consent was obtained from each patient. A total of 115 gallbladder tissue specimens including 105 paraffin-embedded specimens (85 GBC, 10 gallbladder precancerous or benign lesion specimens) and 10 fresh GBC specimens confirmed by operation and histopathology were used in this study. All GBC patients had not received chemotherapy or radiotherapy before surgery. Curative resection (R0 resection) was defined as no residual tumor status, whereas microscopic (R1 resection) and macroscopic residual tumor (R2 resection) was defined as non-curative resection. To reduce effects directly related to surgery, patients who died within one month after surgical resection were not included. Two independent pathologists who blinded to the patients' clinical status verified diagnoses of these GBC samples. According to WHO criteria and the Nevin stage system, detailed clinicopathological and follow-up data were collected from the patient's medical records and completed by a telephone survey, routine visit record and address. Clinical outcome was followed from the date of surgery to the date of death or until the end of September 30, 2011. Cases lost during follow-up were regarded as censored data for the survival analysis. The median follow-up period for all patients was 18.6 (range, 1–60) months. The 5-year overall survival (OS) rate was 11.8% (10/85). Demographic and clinicopathological data are summarized in Table 1.

Table 1
Correlation between NOX4 expression in tumor cells and clinicopathological parameters in patients with gallbladder cancer.

Variable	NOX4 expression [n (%)]		x^2 value	Spearman rank correlation, r(*P*)
	Low	High	(*P*)	
Age (y)	13(40.6)	19(59.4)	0.127(0.649)	0.013 (0.834)
> 65	23(43.3)	30(56.7)		
≤ 65				
Gender	26(52)	24(48)	1.153(0.361)	0.244 (0.120)
Male	12(34.2)	23(65.8)		
Female				
Tumor location	20(47.6)	22(52.4)	0.689(0.388)	0.105 (0.505)
Bottom	15(34.9)	28(65.1)		
Neck and other				
Tumor size (cm)	19(42.2)	26(57.8)	0.734(0.289)	0.125(0.434)
> 3	19(47.5)	21(52.5)		
≤ 3				
Histological types	29(35.8)	52(64.2)	0.093(0.672)	0.272(0.345)
Adenocarcinoma	1(25)	3(75)		
Other [a]				
Differentiation degree	7(63.6)	4(36.4)	7.676(0.018) [b]	0.422 (0.004) [b]
High	16(47)	18(53)		
Moderate	8(20)	32(80)		
Poor				
Liver metastases	15(33.3)	30(66.7)	4.715(0.030) [b]	0.334 (0.032) [b]
(+)	21(52.5)	19(47.5)		
(-)				
Vascular invasion	13(27)	35(73)	5.904(0.025) [b]	0.352 (0.028) [b]
(+)	15(40.5)	22(59.5)		
(-)				

Variable	NOX4 expression [n (%)]		x^2 value	Spearman rank correlation, r(*P*)
	Low	High	(*P*)	
Lymph node metastasis	15(33.3)	30(66.7)	1.656(0.198)	0.053 (0.635)
(+)	19(47.5)	21(52.5)		
(-)				
Nevin staging	21(32.8)	43(67.2)	6.125(0.019) [b]	0.382 (0.025) [b]
III, IV, V	10(47.6)	11(52.4)		
I, II				
Resection method	14(32.5)	29(67.5)	1.660(0.202)	0.055 (0.644)
R1, R2	20(47.6)	22(52.4)		
R0				
VM	18(81.8)	4(18.2)	6.625(0.017) [b]	0.321 (0.016) [b]
(+)	12(19.1)	51(80.9)		
(-)				

[a]: squamous cell carcinoma, adenosquamous carcinoma; [b]: $P < 0.05$: statistically significant.

Affymetrix chip analysis on the gene expression profile for GCAFs/NFs and VM (+)/ VM (-) in vitro

Affymetrix GeneChip Human 1.0ST array (Affymetrix, USA) was used to analyze the gene expression profile in GCAFs/NFs *in vitro*. Briefly, after extracting total RNA in triplicate from GCAFs/NFs and testing the quality, 130 μl of the IVT Master Mix was added into to 130 μl of double-stranded cRNA using a GeneChip 3'IVT PLUS Kit (Affymetrix, USA) to perform RNA RT and *in vitro* transcription (IVT) of cRNA. Then the newly generated cRNA was synthesized, purified and labeled. Finally, after hybridizing and cleaning with a GeneChip Hybridization Wash and Stain kit (Affymetrix, USA), the Genechip Array scanner 3000 (Affymetrix, USA) was used to scan the assays to find out the differentially expressed genes between GCAFs and NFs. Array data were normalized by log scale robust multi-array analysis and analyzed by R-Project software. The gene expression was considered significant if the fold change (FC) value was > 1.5 or < 0.67, and $P < 0.05$. Gene Ontology (GO) analysis was used for functional enrichment analysis, and gene set enrichment analysis and Fisher exact analysis were used to perform statistical analysis of GO. In order to explore the differences of gene expression profile between GCAFs and NFs, potentially relevant up- or down-regulated genes involved in biological processes were selected for verification.

Affymetrix Human lncRNA array (Affymetrix, USA) was used to analyze the expression profile of VM related genes in VM (+) and VM (-) groups *in vitro*. Transcriptome library construction, transcriptome assembly and annotation protocols were provided by Shanghai Oe Biotech Co., Ltd., China. The Pearson correlation between its expression value and each mRNAs expression value was calculated for each lncRNA. For function prediction of lncRNAs, the co-expressed mRNAs for each differentiated lncRNA were calculated and then a functional enrichment analysis of this set of co-expressed mRNAs was carried out. The enriched functional terms were used as the predicted functional term of given lncRNA. The co-expressed mRNAs of lncRNAs were identified by calculating Pearson correlation with correlation *P*-value < 0.05. Then the hypergeometric cumulative distribution function was used to calculate the enrichment of functional terms in annotation of co-expressed mRNAs. The cis-regulation regions were identified by the following procedures. For each lncRNAs, we identified the mRNAs as "cis-regulated mRNAs" when: (1) the mRNAs loci are within 300 k windows up- and down-stream of the given lncRNA, (2) the Pearson correlation of lncRNA-mRNA expression is significant (*P*-value of correlation ≦ 0.05).

Immunohistochemistry (IHC) and enzyme-linked immunosorbent assay (ELISA) in vitro **and** in vivo

IHC was used to detect the expression of NOX4 protein in sections from the 3-D co-culture samples *in vitro*, nude mice xenografts *in vivo* and human gallbladder tissues or stroma. After deparaffinizating and inactivating endogenous peroxides, the sections (4 μm thick) were pretreated with bovine serum albumin V working solution (Beijing Solarbio Science &Technology Co., China), then incubated with primary anti-rabbit NOX4 (Sigma, USA), secondary anti-rabbit IgG (Maixin, China) and 3, 3-diaminobenzidine (DAB) solution, and stained with hematoxylin according to the manufacturer's instructions. Phosphate buffer saline (PBS; Thermo Fisher Scientific, USA) was used to replace the primary antibody for negative control. The expression of NOX4 was observed under an optical microscope (Olympus, Japan). In order to score the stains, five random fields of each section were observed or more than 500 cells counted per slide. In addition, the expression of NOX4 in different human gallbladder tissue/stroma was evaluated by a semi-quantitative system with the staining index (SI). The SI scoring criteria are as follows: (positive cell percentage score) (staining intensity score). The positive cell percentage was scored from 0 to 4 as follows: 0 (no positive cells), 1 (1%-25%), 2 (26%-50%), 3 (51%-75%) and 4 (76%-100%). The staining intensity was scored from 0 to 3 as follows: 0 (negative), 1 (weak), 2 (moderate), and 3 (strong). 3 of SI score were used to distinguish between low (IS ≤ 3) and high (IS > 3) protein expression.

The expression of interleukin-6 (IL-6) protein product in supernatant from the 3-D co-culture samples *in vitro* or nude mice xenografts *in vivo* was determined by ELISA using the Human IL-6 ELISA Kit (Abcam, UK) according to the manufacturer's protocol. All samples were analyzed in triplicate.

Co-immunofluorescence (CIF) staining in vivo

CIF staining with stromal markers such as α-SMA and FSP-1 was used to confirm the expression of NOX4 in GBC stroma. The above IHC samples were permeabilized in PBS containing 10% methanol for 30 min, washed in PBS, and sealed with PBS containing 3% FBS for 1 h. The M.O.M kit (Vector Laboratories, Inc., USA) was used to block Mouse IgG according to the manufacturer's instruction. For CIF staining of NOX4

and α-SMA or FSP1, the sections were respectively incubated with rabbit anti-NOX4 (1:500; GeneTex, USA) and mouse anti-α-SMA (1:200; Abcam, UK) or mouse anti-FSP-1 (1:100; Abcam, UK) at 4 ˚C overnight. Then, the sections were incubated with corresponding secondary antibodies, goat anti-rabbit IgG (1:1,000; Abcam, UK) for detecting NOX4 expression, goat anti-mouse IgG (1:200; Abcam) for α-SMA, goat anti-rabbit IgG (1:200; Abcam) for FSP1. Finally, the sections were washed in PBS and stained with diamidine phenylindole (DAPI) for 5 min, and observed under an immunofluorescence microscope.

qRT-PCR in vitro

Quantitative reverse transcription-polymerase chain reaction (qRT-PCR) was used to verify the different expression of NOX4 at mRNA level in GCAFs/NFs and the expression of JAK1, JAK2 and STAT3 mRNAs of the IL-6/JAK/STAT3 signal pathway genes in GCAFs-triggered VM formation of GBC cells *in vitro*. Total RNA was extracted from cultured or co-cultured cells by Trizol reagent (Thermo Fisher Scientific, USA). GAPDH primers were used as the control for PCR amplification. The gene-specific primer sequences of NOX4, IL-6/JAK/STAT3 signal pathway genes and housekeeping gene GAPDH were as follows: NOX4, Forward: 5'-GTG TCT AAG CAG AGC CTC AGC ATC-3', Reverse: 5'-CGG AGG TAA GCC AAG AGT GTT CG-3'; IL-6, Forward: 5'-GTG GAC CTG ACC TGC CGT CTAG-3', Reverse: 5'-GAG TGG GTG TCG CTG TTG AAG TC-3'; JAK1, Forward: 5'-CAT CGT GAT CTT GCT GCT CAG-3', Reverse: 5'-ACT CCI TGA TGC ACC ATA CGT C-3'; JAK2, Forward: 5'-TCC TCA GAA CGT TGA TGG CAG-3', Reverse: 5'-ATT GCT TTC CTT TTT CAC AAG AT-3'; STAT3, Forward: 5'-GAG AAG GAC ATC AGC GGT AAG-3’, Reverse: 5'-AGT GGA GAC ACC AGG ATA TTG-3’; GAPDH, Forward: 5'CTC CTC CTG TTC GAC AGT CA3', Reverse: 5'GCT CCG CCC AGA TAC CATT3'. The PCR amplification reaction was as follows: 94˚C for 3 min, followed by 40 cycles of 95˚C for 15 s, 60˚C for 30 s, 72˚C for 30 s, and 82–86˚C (fluorescence collection) for 5–10 s, and finally 72–99˚C for 5 min. The PCR product (10 μl) was placed on 15 $g \cdot l^{-1}$ agarose gel and observed by ethidium bromide (Cusabio Biotech, China) staining with ABI-Prism 7300 SDS software (Bio-Rad Laboratories, USA).

Western blotting in vitro **and** in vivo

Western blotting was used to verify the expression of NOX4 protein and the expression of IL-6, JAK1, JAK2 or STAT3 protein in the 3-D culture/co-culture samples *in vitro* and nude mice xenografts *in vivo*. The total protein was isolated from the 3-D culture/co-culture samples and nude mice xenografts with RIPA (radioimmunoprecipitation assay) Lysis Buffer (SBJBIO, China), and the concentration was detected using BCA protein assay kit (Kangchen BioTech, China). Then, an aliquot of 20 μg proteins was subjected to 10% SDS-PAGE (sodium dodecyl sulfate-polyacrylamide gel electrophoresis) under reducing conditions, and proteins were transferred to a PVDF (polyvinylidene difloride) membrane (Millipore, USA). The membrane was incubated with the primary rabbit anti-NOX4 antibody (1:3000; Abcam, UK), anti-IL-6 antibody (1:3000; KangChen Biotech, China, the same below), anti-JAK1 antibody(1:2000), anti-JAK2 antibody (1:2000), anti-STAT3 antibody (1:1500) and mouse anti-human β-actin antibody (1:1000), and then the appropriate dose of horseradish peroxidase labeled anti-mouse/rabbit secondary antibody (1:1000; Kangchen BioTech) was added for further incubation. The target proteins were displayed by an enhanced chemiluminescent (ECL) kit (Kangchen BioTech), and imaged on a chemiluminescence imager.

The gray value and gray coefficient ratio of every protein were analyzed and calculated with Image J analysis software (National Institutes of Health).

Statistical analysis

All data were expressed as mean ± SD (standard deviation), and statistically analyzed by SPSS 22.0 software (IBM, USA). The SI was analyzed using Kruskall-Wallis test with Dunn's post-hoc comparison. Student *t*-test was used in independent sample analysis. The χ^2 test was used to analyze the relationship between NOX4 expression and GBC patients' clinicopathologic parameters. Bivariate correlations between two independent variables were analyzed by calculating the Spearman's correlation coefficients. The survival analysis was calculated by Kaplan Meier method and compared by log rank test. The Cox's regression model was used for univariate and multivariate analysis of prognostic factors. $P < 0.05$ was considered to be statistically significant.

Results

GCAFs promote VM formation of GBC cells in vitro

A 3-D co-culture system of GBC-SD and GCAFs/NFs was established to investigate the effect of GCAFs on the VM formation of GBC. As showed in Fig. 1, GBC-SD cells and GBC-SD + NFs groups formed vasculogenic-like networks when cultured on Matrigel and rat-tail collagen-matrix for 2 days, and had VM formation for 14 days; but GBC-SD + GCAFs group formed patterned vasculogenic-like networks for only 19 hours, had VM formation for only one week; and the tube number of vasculogenic-like networks in GBC-SD + GCAFs was significantly more than that of alone GBC-SD cells and GBC-SD + NFs ($P < 0.05$). Furthermore, PAS positive, cherry-red materials found in granules and patches in the cytoplasm of GBC-SD cells appeared around the signal cell or cell clusters. These results showed that GCAFs can promote VM formation of GBC-SD cells *in vitr*o.

GCAFs promote the proliferation, invasion, migration and tube formation of GBC cells in vitro

To verify that GCAFs promote VM formation of GBC cells, we detected malignant phenotypes including proliferation, invasion, migration and tube formation of GBC cells triggered by GCAFs *in vitro* using a co-culture model of GBC cells (GBC-SD, SGC-996, TJ-GBC2) and fibroblasts (GCAFs, NFs). As shown in Fig. 2, the proliferation ability of GBC cell + GCAFs groups were significantly enhanced compared to alone GBC cell or GBC cell + NFs groups (all $P < 0.05$; Fig. 2A); the number (relative invasive ability) of cells that invaded the basement membrane in GBC cell + GCAFs groups was significantly more than that of alone GBC cell or GBC cell + NFs groups (all $P < 0.05$; Fig. 2B); the cell migration rate in GBC cell + GCAFs co-culture groups was significantly higher than that of alone GBC cell groups or GBC cell + NFs co-culture groups (all $P < 0.05$; Fig. 2C). Furthermore, tube formation assay showed that tube structure was observed in HUVEC + GBC-SD + GCAFs groups at 12 h; no obvious tube structure was seen in HUVECs or HUVEC + GBC-SD + NFs cultured in Matrigel for 12 h, and the formation of tube structure cannot be observed until about 18 h. At 48 h, obvious tube formation was observed in HUVEC, HUVEC + GBC-SD, HUVEC + GBC-SD

+ NFs and HUVEC + GBC-SD + GCAFs groups; but among them, the number of the lumen formed in HUVEC + GBC-SD + GCAFs group was significantly more than that of the other three groups (all $P < 0.01$; Fig. 2D). Taken together, GCAFs can promote the proliferation, invasion, migration and tube formation of GBC cells/HUVECs, and then promote VM formation.

GCAFs promote VM formation and tumor growth of GBC xenografts in vivo

A nude mouse xenograft model was established to further verify whether GCAFs can promote VM formation and tumor growth of GBC *in vivo*. As shown in Fig. 3, size, volume and growth curves of tumor xenografts in GBC-SD + GCAFs groups were significantly larger than that of GBC-SD group ($P < 0.05$; Fig. 3A); H&E staining (Fig. 3Bb1) and CD_{31}-PAS double staining (Fig. 3Bb2) of xenografts section in GBC-SD and GBC-SD + GCAFs groups showed that tumor cells were lined with vessel-like structure, with single or multiple red blood cell inside, without any evidence of tumor necrosis, and PAS positive substances were arranged in a channel-like arrangement; furthermore, TEM (Fig. 3Bb3) clearly visualized single or multiple red blood cells in the central of tumor nests in the xenografts; but the number of blood vessel-like structures, erythrocytes and PAS positive substances in GBC-SD + GCAFs group were significantly more than those of GBC-SD group (Fig. 3Bb1-2). These results further confirmed that GCAFs have the ability to promote tumor growth and VM formation in GBC.

NOX4, as a GCAFs-derived VM-related gene, is highly expressed in the process of VM formation in GBC triggered by GCAFs

In order to understand which genes are involved in the VM formation triggered by GCAFs in GBC, we analyzed the gene difference expression profile of GCAFs/NFs and VM(+)/VM(-) *in vitro* using Affymetrix GeneChip Human 1.0ST array and Affymetrix Human lncRNA array. As shown in Fig. 4, a total of 466 upregulated genes (FC > 1.5) and 596 downregulated genes (FC < 0.67) were identified in GCAFs/NFs according to the inclusion criteria. As one of 16 angiogenesis-related genes, NOX4 was significantly upregulated (FC = 2.58) in GCAFs compared with NFs. Furthermore, Affymetrix Human lncRNA array was used to analyszed VM-related gene expression profile in GBC. Venn modal analysis (upregulation, > 2 times; or downregulation, < 0.5 times) showed that the expression of NOX4, JAK and STAT3 was significantly upregulated in 154 VM-related genes (Fig. 5). These data preliminary showed that NOX4, as a GCAFs-derived VM-related gene, is highly expressed in the progress of VM formation triggered by GCAFs in GBC.

To verify that NOX4 expression is upregulated during the formation of VM induced by GCAFs in GBC, we further detected the expression of NOX4 *in vitro* and *in vivo* using qRT-PCR, western blot and IHC. As shown in Fig. 6, NOX4 mRNA expression in GCAFs (Fig. 6A.a1) or in 3-D matrices of GBC cell (GBS-SD, SGC-996, OCUG-1) + GCAFs co-culture (Fig. 6a2) was significantly upregulated compared with NFs or alone GBC cells *in vitro*, which was consistent with the results of microarray analysis. And, the expression of NOX4 protein in GBC cell + GCAFs co-culture groups was significantly higher than that of GBC-SD + NFs co-culture or alone GBC-SD *in vitro* (all $P < 0.05$; Fig. 6A.a3-4), but no statistical difference was

observed between GBC-SD + NFs and GBC-SD groups. Furthermore, the expression of NOX4 in GBC xenografts *in vivo* was detected by IHC (Fig. 6B.b1) and western blotting (Fig. 6B.b2). The results showed that NOX4 was also high expressed in GBC-SD + GCAFs group compared with GBC-SD group (all $P < 0.05$); and the expression of NOX4 mRNA in GBC-SD + GCAFs group was significantly upregulated compared with GBC-SD group ($P < 0.05$; Fig. 6B.b3). All together, these data verified that NOX4, as a GCAFs-derived VM-related gene, was highly expressed in VM formation triggered by GCAFs; in other words, GCAFs upregulated NOX4 expression in the process of VM formation in GBC.

To further verify whether NOX4 was over-expressed in VM formation of GBC triggered by GCAFs, we detected the expression of NOX4 protein in human gallbladder tissue or stroma samples using IHC and CIF staining. As shown in Fig. 7, the staining index (SI) of NOX4 expression (cytoplasmic and/or nuclear brown staining) in GBC epithelium or stroma was significantly higher than that in gallbladder precancerous lesions (epithelium: 5.471 ± 0.410 *vs*. 1.900 ± 0.348, $P = 0.007$; stroma: 5.965 ± 0.419 *vs*. 2.000 ± 0.394, $P = 0.003$) and benign lesions (epithelium: 5.471 ± 0.410 *vs*. 1.100 ± 0.379; stroma: 5.965 ± 0.419 *vs*. 1.700 ± 0.396; both $P = 0.001$), but there was no significant difference in the expression of NOX4 between precancerous and benign lesions (P = 0.863) or stroma (P = 0.980) (Fig. 7A). In addition, CIF staining with stromal markers α-SMA and FSP-1 showed that NOX4 (green) overlapped or co-localized with α-SMA and FSP1 (red or brown) positive stroma in GBC (Fig. 7B). These results further confirmed that NOX4, as a key gene for VM formation, was over-expressed in GBCs-induced VM formation of GBC.

NOX4 is related to aggression and unfavorable prognosis of GBC patients

Here, We further discussed the relationship between NOX4 expression and clinical, pathological and prognostic factors in GBC patients. SI score was used to distinguish NOX4 expression: IS ≤ 3, NOX4 low expression; >3, high expression. In the tumor cells of GBC, NOX4 was highly expressed in 50 cases (58.8%) and low in 35 cases (41.2%); in stromal cells, the expression of NOX4 was high in 55 cases (64.7%) and low in 30 cases (35.3%). As shown in Table 1–2, chi-square analysis and spearman rank correlation analysis indicated that the expression of NOX4 in tumor/stromal cells was not related to age, gender, tumor location, tumor size, histological type, lymph node metastasis and resection method (all $P > 0.05$), but significantly associated with tumor differentiation, liver metastasis, vascular invasion, Nevin staging and VM (all $P < 0.05$) in GBC patients.

Table 2
Correlation between NOX4 expression in tumor stroma and clinicopathological parameters in patients with gallbladder cancer.

Variable	NOX4 expression [n (%)]		x^2 value	Spearman rank correlation, r(*P*)
	Low	High	(*P*)	
Age (y)	13(40.6)	19(59.4)	0.127(0.649)	0.013 (0.834)
> 65	23(43.3)	30(56.7)		
≤ 65				
Gender	26(52)	24(48)	1.153(0.361)	0.244 (0.120)
Male	12(34.2)	23(65.8)		
Female				
Tumor location	20(47.6)	22(52.4)	0.689(0.388)	0.105 (0.505)
Bottom	15(34.9)	28(65.1)		
Neck and other				
Tumor size (cm)	19(42.2)	26(57.8)	0.734(0.289)	0.125(0.434)
> 3	19(47.5)	21(52.5)		
≤ 3				
Histological types	29(35.8)	52(64.2)	0.093(0.672)	0.272(0.345)
Adenocarcinoma	1(25)	3(75)		
Other [a]				
Differentiation degree	7(63.6)	4(36.4)	7.676(0.018) [b]	0.422 (0.004) [b]
High	16(47)	18(53)		
Moderate	8(20)	32(80)		
Poor				
Liver metastases	15(33.3)	30(66.7)	4.715(0.030) [b]	0.334 (0.032) [b]
(+)	21(52.5)	19(47.5)		
(-)				
Vascular invasion	13(27)	35(73)	5.904(0.025) [b]	0.352 (0.028) [b]
(+)	15(40.5)	22(59.5)		
(-)				

Variable	NOX4 expression [n (%)]		x^2 value	Spearman rank correlation, r(*P*)
	Low	High	(*P*)	
Lymph node metastasis	15(33.3)	30(66.7)	1.656(0.198)	0.053 (0.635)
(+)	19(47.5)	21(52.5)		
(-)				
Nevin staging	21(32.8)	43(67.2)	6.125(0.019) [b]	0.382 (0.025) [b]
III, IV, V	10(47.6)	11(52.4)		
I, II				
Resection method	14(32.5)	29(67.5)	1.660(0.202)	0.055 (0.644)
R1, R2	20(47.6)	22(52.4)		
R0				
VM	18(81.8)	4(18.2)	6.625(0.017) [b]	0.321 (0.016) [b]
(+)	12(19.1)	51(80.9)		
(-)				

[a]: squamous cell carcinoma, adenosquamous carcinoma; [b]: $P < 0.05$: statistically significant.

Furthermore, the Cox proportional hazard model was used to determine the influencing factors related to survival prognosis, i.e. OS rate of GBC patients (Table 3). The univariate analysis suggested that tumor histological type, differentiation degree, Nevin stage, liver metastasis, vascular invasion, lymph node metastasis, resection method, NOX4 expression in tumor cells/GCAFs were significant prognostic indicators for the OS of GBC patients (all $P < 0.05$). Therefore, these indicators were selected as parameters to be included in the same Cox regression model. Further multivariate analysis confirmed that differentiation degree, liver metastasis, vascular invasion and NOX4 stroma expression (all $P < 0.05$) were the independent prognostic factors for the OS of GBC patients.

Table 3 Cox model analysis of influencing factors of survival prognosis in patients with gallbladder cancer.

Variable	Single factor			Multiple factors		
	HR	95% CI	*P*	HR	95% CI	*P*
Gender						
Male vs. female	0.972	0.609-1.554	0.907			
Age (y)						
>65 *vs.* ≤65	0.808	0.517-1.262	0.348			
Tumor site						
Bottom vs. neck etc.	0.755	0.481-1.184	0.221			
Tumor size (cm)						
>3.0 *vs.* ≤3.0	1.434	0.909-2.262	0.121			
Histological types						
Adenocarcinoma vs. others [b]	0.255	0.106-0.613	0.002[a]			
Differentiation degree						
High vs. medium/low	0.243	0.114-0.514	0.000[a]	0.437	0.196-0.975	0.039 [a]
Nevin staging						
III~V *vs.* I~II	2.482	1.227-5.021	0.011[a]			
Liver invasion						
(+) *vs.* (-)	2.075	1.294-3.327	0.002[a]	1.949	1.187-3.201	0.012 [a]
Vascular invasion						
(+) *vs.* (-)	3.235	1.911-5.475	0.000[a]	2.569	1.486-4.444	0.003 [a]
Lymph node metastasis						
(+) *vs.* (-)	1.708	1.057-2.762	0.029[a]			

Resection method						
R1, R2 *vs.* R0	0.413	1.672-5.041	0.000[a]			
NOX4 expression in cancer cells						
High *vs.* low	1.985	1.484-3.592	0.005[a]			
NOX 4 expression in stroma cells						
High *vs.* low	1.628	1.389-3.329	0.035[a]	1.767	1.062-3.942	0.022 [a]

[a] $P < 0.05$, statistically significant;

[b]: adenocarcinoma, squamous cell carcinoma, adenosquamous carcinoma; HR, Hazard ratio; CI, confidence interval.

Finally, Kaplan-Meier analysis and the log-rank test were used to further evaluate the effect of NOX4 expression on the survival of GBC patients. The mean, median and a 5-year survival rate for survival time of the high NOX4 expression in tumor cells (50/85, 58.8%) were 15.6 and 5.8 months and 10.5%, compared with 30.5 and 25.0 months and 22.2% for the low NOX4 expression (35/85, 41.2%). The mean, median and a 5-year survival rate for survival time of the high NOX4 expression in GBC stroma (55/85, 64.7%) were 15.7 and 4.8 months and 10.3%, compared with 26.7 and 16.1 months and 19.4% for the low NOX4 expression (30/85, 35.3%). As shown in Fig. 7C, Kaplan-Meier analysis showed that the survival time of GBC patients with high NOX4 expression in GBC tumor (Fig. 7C1, $P = 0.026$) and stroma (Fig. 7C2, $P = 0.020$) was significantly shorter than that of GBC with low NOX4 expression.

All together, these results confirmed that the expression of NOX4, especially in the tumor stroma, is an independent prognostic factor of GBC. The high expression of NOX4 in GBC tumor/stroma is closely related to VM formation, and indicates poor prognosis.

GCAFs promote VM formation of GBC via upregulating NOX4 expression through IL-6/JAK/STAT3 signaling pathway.

In order to explore the underlying molecular mechanism of GCAFs promoting VM formation of GBC, according to the above experimental results, we constructed a network regulation model of GCAFs promoting VM formation in GBC. As shown in Fig. 8, in this network regulation model, NOX4, STAT3 and JAK were regulated in the VM-related key genes.

Considering that IL-6, which is autocrine-secreted by tumor cells, especially, paracrine-secreted by stromal cells such as CAFs in TME, participates in tumor development by activating of some signal pathways such as STAT3 [33–37], and the IL-6/JAK/STAT3 signaling axis is involved in occurrence and development of cancer [38], we assume that GCAFs promote VM formation in GBC *via* upregulating NOX4

expression through paracrine IL-6 mediating IL-6/JAK/STAT3 signaling pathway. In order to verify the hypothesis, we first detected the expression of IL-6 in GCAFs/NFs *in vitro* using western blotting and ELISA. As shown in Figure 9, IL-6 and its product were highly secreted and upexpressed in the culture supernatant of GCAFs compared with NFs *in vitro* (all $P<0.05$). Furthermore, we detected the expression of related signaling pathway genes in 3-D culture/co-culture matrices using ELISA, western blotting and qRT-PCR. The results showed that the expression of IL-6 product in the supernatant of 3-D co-culture matrices, and the expression of JAK1, JAK2 and STAT3 at protein and mRNA levels in the 3-D co-culture matrices of GBC-SD+GCAFs was significantly higher than that of GBC-SD culture or GBC-SD+NFs co-culture (all $P<0.05$); but no statistical difference was observed in the expression of these genes between GBC-SD and GBC-SD+NFs groups (Figure 10A). Finally, we detected the expression of related signaling pathway genes in the nude mouse xenografts *in vivo* using ELISA, IHC and western blotting (Figure 10B). The results showed that the expression of IL-6 in the supernatant of GBC-SD+GCAFs group was significantly higher than that of GBC-SD group ($P<0.05$), and the protein expression of JAK1, JAK2 and STAT3 in GBC-SD+GCAFs group was significantly higher than that in GBC-SD group (all $P<0.05$). All together, these results suggested that GCAFs promote VM formation of GBC *via* upregulating NOX4 expression through paracrine IL-6 mediating IL-6/JAK/STAT3 signaling pathway.

Discussion

The interaction between TME and tumor cells has been a hotspot in the study of carcinogenesis [4, 5]. CAFs, as the most critical stromal cells in TME, participate in the process of tumor growth and development [6–11, 39]. As an important supplement to tumor microcirculation, VM occurs in certain highly aggressive malignancies, and is closely related to tumor progression and poor prognosis [13–16, 40]. However, the relationship between CAFs and VM formation has rarely been reported. Recently, some studies have confirmed that CAFs can promote VM formation in some tumors, such as HCC [21] and gastric cancer [41, 42]. In this study, we observed that GCAFs can promote VM formation and tumor growth of GBCs *in vitro* and *in vivo*. Therefore, we first believed that GCAFs has the ability to promote tumor growth and VM formation in GBC.

Recently, it was reported that CAFs promote VM formation in HCC cells by secreting TGF-β and SDF1 [21]; CAFs-derived HGF promote vascularization in gastric cancer [41]. So whether there are specific genes regulation in the process of GCAFs-triggered VM formation in GBC? Here, we performed microarray analysis for GCAFs/NFs using Affymetrix GeneChip Human 1.0ST array, and for VM (+)/VM (-) using Affymetrix Human lncRNA array. In the process of analyzing the differentially expressed gene profiles of GCAFs and NFs, we found that 16 genes in GCAFs were related to tumor angiogenesis. Among them, the expression of NOX4 was significantly increased.At the same time, the result of lncRNAs microarray showed that the expression of NOX4, JAK and STAT3 was significantly increased in 154 VM-related genes of GBC. As mentioned above, NOX4, as a member of the NADPH oxidase family, plays vital roles in proliferation, metastasis and angiogenesis of tumors through the production of ROS [29, 43, 44]. Then, we detected NOX4 expression *in vitro* and *in vivo* using qRT-PCR, western blot and IHC. The results showed the expression of NOX4 in GCAFs was significantly up-regulated at both mRNA and protein

levels. Finally, we further detected the expression of NOX4 protein in human gallbladder tissue or stroma samples using IHC and CIF. The results showed NOX4 expression in epithelium or stroma was significantly higher than that in gallbladder precancerous lesions and benign lesions. All together, these data verified the high expression of NOX4 not only in GBC cells/stroma, but also in the process of VM formation induced by GCAFs. In other words, GCAFs upregulate the expression of NOX4 during VM formation in GBC. It has been confirmed that NOX4 is highly expressed in many types of tumor cells such as pancreatic cancer [45], renal cell carcinoma [46] and gastric cancer [47]. However, current researches on NOX4 are mainly focused on tumor cells, and the role of NOX4 in VM formation is rarely mentioned. Thus, our finding firstly confirmed that NOX4 is highly expressed in GBC and its stroma, which is a GCAFs-derived key gene for VM formation.

In order to investigate the clinical value of the overexpression of NOX4, we further studied the relationship between the expression of NOX4 and clinicopathological characteristics/prognostic factors in patients with GBC. It was recently reported that the expression of NOX4 is closely related to the tumor size and prognosis in gastric cancer [47]; the prognosis of colorectal cancer patients with high expression of NOX4 was poor [48]. In this study, the results showed that the high expression of NOX4 in GBC cells, especially in GBC stroma (i.e. GCAFs) was significantly correlated with tumor differentiation, liver metastasis, vascular invasion and Nevin staging, specially VM formation. The multivariate analysis confirmed that tumor differentiation degree, liver metastasis, vascular invasion and NOX4 stroma expression were the independent prognostic factors for the OS of GBC patients. The survival time of GBC patients with high NOX4 expression was significantly shorter than that of GBC patients with low expression. These results firstly confirmed that NOX4 is related with aggression and unfavorable prognosis in patients with GBC; the high expression of NOX4 in GBC and its stroma predicts a poor prognosis.

At present, the mechanism of CAFs promoting tumor VM formation is not clear. It was reported that CAFs promoted VM formation in HCC by paracrine TGF-β and SDF1 [21]; CAFs-derived HGF promoted vascularization in gastric cancer via PI3K/AKT and ERK1/2 signaling [41]; CAFs induced vasculogenic mimicry in gastric cancer cells through the role of EphA2-PI3K signaling [42]. In order to explore the underlying molecular mechanism of GCAFs promoting VM formation in GBC, in view of aforementioned microarray analysis results, we found that among 154 VM-related genes, NOX4, JAK and STAT3 are involved in VM formation of GBC. So, we constructed a gene network regulation model in which GCAFs promote VM formation according to lncRNAs chip analysis. The results showed that JAK1, JAK2, STAT3 and NOX4 were regulated in the VM-related key genes.

Paracrine is one of the important ways in which CAFs act on tumor cells, CAFs can promote tumor cell growth and angiogenesis by secreting a variety of cytokines [31, 32]. It was reported that the JAK/STAT3 signaling pathway plays an important role in mediating the multiple effects of interleukin-6 (IL-6) on tumor proliferation, invasion and metastasis [38]. IL-6 is an important inflammatory cytokine secreted by tumor cells or stromal cells [33], which is highly expressed in some tumors, and participate in a variety of malignant biological processes such as apoptosis, proliferation, metastasis and angiogenesis by activating a variety of signal pathways, such as STAT3, ERK and MAPK [34–37]. So, IL-6/JAK/STAT3

signaling pathway was believed as a key signaling pathway for tumor progression [38], and has been confirmed in many types of solid tumors such as HCC [49], breast cancer [50] and lung adenocarcinomas [51]. Considering that IL-6, which is paracrine-secreted by stromal cells such as CAFs, participates in tumor development by activating the IL-6/JAK/STAT3 signaling axis [38], we assume that GCAFs promote VM formation of GBC *via* upregulating NOX4 expression through paracrine IL-6 mediating IL-6/JAK/STAT3 signaling pathway. In order to verify the hypothesis, we detected the mRNA and protein expression of IL-6, JAK1, JAK2 and STAT3 *in vitro* and *in vivo* using ELISA, IHC, western blotting and qRT-PCR. The results showed that IL-6 was highly secreted and highly expressed in GCAFs, and these pathway genes were highly expressed during the VM formation in GBC. All together, these results firstly suggested that GCAFs promote VM formation in GBC *via* upregulating NOX4 expression through paracrine IL-6 mediating IL-6/JAK/STAT3 signaling pathway.

Conclusions

Collectively, our study firstly demonstrate that GCAFs promote VM formation and tumor growth in GBC *via* upregulating NOX4 expression through paracrine IL-6 mediated IL-6-JAK-STAT3 signal pathway. NOX4, as a key gene of VM formation in GBC, is highly expressed in tumor and stroma, which is related to the progression and poor prognosis of GBC patients. The present findings may be of importance to explore a promising novel strategy for diagnosis, prognostic judge and anti-VM target treatment in human GBC.

Abbreviations

GBC, gallbladder cancer; CAFs, cancer-associated fibroblasts; GCAFs, gallbladder cancer-associated fibroblasts; NFs, normal fibroblasts; VM, vasculogenic mimicry; TME, tumor microenvironment; ECM, extracellular matrix; NOX4, nicotinamide adenine dinucleotide phosphate oxidase 4, NADPH oxidase 4; ROS, reactive oxygen species; DMEM, Dulbecco's modified Eadles medium; HUVEC, human umbilical vein endothelial cell; α-SMA, α-smooth muscle actin; FAP, fibroblast activation protein; IHC, immunohistochemistry; CIF, co-immunofluorescence; FBS, fetal bovine serum; PBS, phosphate buffer saline; CO_2, carbon dioxide; 3-D, three-dimensional; HE, hematoxylin and eosin; PAS, periodic acid-Schiff; DAB, 3,3-diaminobenzidine; OD, optical density; SPF, specific pathogen-free; TEM, transmission electron microscopy; OS, overall survival; IVT, *in vitro* transcription; FC, fold change; GO, Gene Ontology; SI, staining index; ELISA, enzyme-linked immunosorbent assay; IL-6, interleukin-6; DAPI, diamidine phenylindole; qRT-PCR, quantitative reverse transcription-polymerase chain reaction; JAK, Janus kinase; STAT, signal transducer and activator of transcription; GAPDH, glyceraldehyde-3-phosphate dehydrogenase; RIPA, radioimmunoprecipitation assay; ECL, enhanced chemiluminescent; HR, Hazard ratio; CI, confidence interval.

Declarations

Ethics approval and consent to participate

This study was approved by the Ethics Committee and the Institutional Review Board at the Tongji Hospital. All patients provided written informed consent.

Consent for publication

Not applicable.

Availability of data and materials

The datasets and materials used during the current study are available from the corresponding author on reasonable request.

Competing interests

The authors declare that they have no competing interests.

Funding

This work was supported by funds from the National Nature Science Foundation of China (Nos. 30672073, 81072004 and 81372614), the Natural Science Foundation Project in Shanghai (No.13ZR1432300) and the Shanghai Science and Technology Commission Research Project (Nos. 19411966300 and 19140902302).

Authors' contributions

Pan MS, Sun W and Fan YZ designed the research, analyzed the data and wrote the manuscript. Pan MS, Ansari KH and Sun W carried out *in vitro* experiments and 3-D culture of GBC-SD cells. Pan MS, Wang H carried out *in vivo* experiments of nude mouse xenografts and clinical detection. Fan YZ is the guarantor. All authors have read and approved the final manuscript.

Acknowledgements

This work was supported by funds from the National Nature Science Foundation of China (Nos. 30672073, 81072004 and 81372614), the Natural Science Foundation Project in Shanghai

(No.13ZR1432300) and the Shanghai Science and Technology Commission Research Project (Nos. 19411966300 and 19140902302). We would like to thank Professor Ying-Bin Liu at the Shanghai Xinhua Hospital and Professor Yao-Qin Yang at the Tongji University School of Medicine (Shanghai, China) for their generous gifts of gallbladder cancer OCUG-1 and SGC-996 cell lines in this study.

References

1. McNamara MG, Metran-Nascente C, Knox JJ. State-of-the-art in the management of locally advanced and metastatic gallbladder cancer. Curr Opin Oncol. 2013;5:425–31.
2. Stern MC, Fejerman L, Das R, Setiawan VW, Cruz-Correa MR, Perez-Stable EJ, et al. Variability in cancer risk and outcomes within US latinos by national origin and genetic ancestry. Curr Epidemiol Rep. 2016;3:181–90.
3. Nakamura H, Arai Y, Totoki Y, Shirota T, Elzawahry A, Kato M, et al. Genomic spectra of biliary tract cancer. Nat Genet. 2015;47:1003–10.
4. Liotta LA, Kohn EC. The microenvironment of the tumor-host interface. Nature. 2001;411:375–9.
5. Quail DF, Joyce JA. Microenvironmental regulation of tumor progression and metastasis. Nat Med. 2013;19:1423–37.
6. Kobayashi H, Atsushi E, Woods SL, Burt AD, Takahashi M, Worthley D. Cancer-associated fibroblasts in gastrointestinal cancer. Nat Rev Gastroenterol Hepatol. 2019;16:282–95.
7. Kharaishvili G, Simkova D, Bouchalova K, Gachechiladze M, Narsia N, Bouchal J. The role of cancer associated fibroblasts, solid stress and other microenvironmental factors in tumor progression and therapy resistance. Cancer Cell Int. 2014;14:41.
8. Yamamura Y, Asai N, Enomoto A, Kato T, Mii S, Kondo Y, et al. Akt-Girdin signaling in cancer-associated fibroblasts contributes to tumor progression. Cancer Res. 2015;75:813–23.
9. Orimo A, Gupta PB, Sgroi DC, Arenzana-Seisdedos F, Delaunay T, Naeem R, et al. Stromal fibroblasts present in invasive human breast carcinomas promote tumor growth and angiogenesis through elevated SDF-1/CXCL12 secretion. Cell. 2005;121:335–48.
10. Wang FT, Sun Wei, Zhang JT, Fan YZ. Cancerassociated fibroblast regulation of tumor neoangiogenesis as a therapeutic target in cancer. Oncol Lett. 2019;17:3055–65.
11. Wang FT, Mohamed MH, Ansari KH, Xu GL, Li XP, Fan YZ. Upregulated NOX1 expression in gallbladder cancer associated fibroblasts predicts a poor prognosis. Oncol Rep. 2019;42:1475–86.
12. Folkman J. Angiogenesis in cancer, vascular, rheumatoid and other disease. Nature Med. 1995;1:27–30.
13. Maniotis AJ, Folberg R, Hess A, Seftor EA, Gardner LM, Pe'er J, et al. Vascular channel formation by human melanoma cells in vivo and in vitro: vasculogenic mimicry. Am J Pathol. 1999;155:739–52.
14. Fan YZ, Sun W, Zhang WZ, Ge CY. Vasculogenic mimicry in human primary gallbladder carcinoma and clinical significance thereof. Nalt Med J China. 2007;87:145–9.

15. Sun W, Fan YZ, Zhang WZ, Ge CY. A pilot histomorphology and hemodynamic of vasculogenic mimicry in gallbladder carcinomas *in vivo* and *in vitro*. J Exp Clin Cancer Res. 2011;30:46–58.
16. Sun W, Shen ZY, Zhang H, Fan YZ, Zhang WZ, Zhang JT, Lu XS, Ye C. Overexpression of HIF-1α in primary gallbladder carcinoma and its relation to vasculogenic mimicry and unfavorable prognosis. Oncol Rep. 2012;27:1990–2002.
17. Fan YZ, Sun W. Molecular regulation of vasculogenic mimicry in tumors and potential tumor-target therapy. World J Gastroint Surg. 2010;2:117–27.
18. Zhang JT, Sun W, Zhang WZ, Ge CY, Liu ZY, Zhao ZM, Lu XS, Fan YZ. Norcantharidin inhibits tumor growth and vasculogenic mimicry of human gallbladder carcinomas by suppression of the PI3-K/MMPs/Ln-5γ^2 signaling pathway. BMC Cancer. 2014;14:193.
19. Wang H, Sun W, Zhang WZ, Ge CY, Zhang JT, Liu ZY, Fan YZ. Inhibition of tumor vasculogenic mimicry and prolongation of host survival in highly aggressive gallbladder cancers by norcantharidin *via* blocking the ephrin type a receptor 2/focal adhesion kinase/Paxillin signaling pathway. PLoS One. 2014;9:e96882.
20. Zhu W, Sun W, Zhang JT, Liu ZY, Li XP, Fan YZ. Norcantharidin enhances TIMP-2 anti-vasculogenic mimicry activity for human gallbladder cancers through downregulating MMP-2 and MT1-MMP. Int J Oncol. 2015;46:627–40.
21. Yang J, Lu Y, Lin YY, Zheng ZY, Fang JH, He S, et al. Vascular mimicry formation is promoted by paracrine TGF-β and SDF1 of cancer-associated fibroblasts and inhibited by miR-101 in hepatocellular carcinoma. Cancer Lett. 2016;383:18–27.
22. Ansari KH, Fan YZ. NADPH oxidase 4 (NOX4) and Cancer. Eur J Pharm Med Res (EJPMR). 2019;6:6548.
23. Trachootham D, Alexandre J, Huang P. Targeting cancer cells by ROS-mediated mechanisms: a radical therapeutic approach. Nat Rev Drug Discov. 2009;8:579–91.
24. Meitzler JL, Antony S, Wu Y, Juhasz A, Liu H, Jiang G, et al. NADPH oxidases: a perspective on reactive oxygen species production in tumor biology. Antioxid Redox Signal. 2014;20:2873–89.
25. Roy K, Wu Y, Meitzler JL, Juhasz A, Liu H, Jiang G, et al. NADPH oxidases and cancer. Clin Sci. 2015;128:863–75.
26. Wu Y, Antony S, Meitzler JL, Doroshow JH. Molecular mechanisms underlying chronic inflammation-associated cancers. Cancer Lett. 2014;345:164–73.
27. Jayavelu AK, Müller JP, Bauer R, Böhmer SA, Lässig J, Cerny-Reiterer S, et al. NOX4-driven ROS formation mediates PTP inactivation and cell transformation in FLT3ITD-positive AML cells. Leukemia. 2016;30:473.
28. You X, Ma M, Hou G, Hu Y, Shi X. Gene expression and prognosis of NOX family members in gastric cancer. OncoTargets Therapy. 2018;11:3065.
29. Helfinger V, Henke N, Harenkamp S, Walter M, Epah J, Penski C, et al. The NADPH Oxidase Nox4 mediates tumour angiogenesis. Acta Physiol (Oxf). 2016;216:435–46.

30. Liu ZY, Xu GL, Tao HH, Yang YQ, Fan YZ. Establishment and characterization of a novel highly aggressive gallbladder cancer cell line, TJ-GBC2. Cancer Cell Int. 2017;17:20.
31. Ilkow CS, Marguerie M, Batenchuk C, Mayer J, Neriah DB, Cousineau S, et al. Reciprocal cellular cross-talk within the tumor microenvironment promotes oncolytic virus activity. Nat Med. 2015;21:530–6.
32. Hanahan D, Coussens LM. Accessories to the crime: functions of cells recruited to the tumor microenvironment. Cancer Cell. 2012;21:309–22.
33. Hunter CA, Jones SA. IL-6 as a keystone cytokine in health and disease. Nat Immunol. 2015;16:448–57.
34. Mauer J, Denson JL, Brüning JC. Versatile functions for IL-6 in metabolism and cancer. Trends Immunol. 2015;36:92–101.
35. Rossi JF, Lu ZY, Jourdan M, Klein B. Interleukin-6 as a therapeutic target. Clin Cancer Res. 2015;21:1248–57.
36. He GB, Dhar D, Nakagawa H, Font-Burgada J, Ogata H, Jiang YH, et al. Identification of liver cancer progenitors whose malignant progression depends on autocrine IL-6 signaling. Cell. 2013;155:384–96.
37. Shinriki S, Jono H, Ueda M, Ota K, Ota T, Sueyoshi T, et al. Interleukin-6 signalling regulates vascular endothelial growth factor-C synthesis and lymphangiogenesis in human oral squamous cell carcinoma. J Pathol. 2011;225:142–50.
38. Johnson DE, O'Keefe RA, Grandis JR. Targeting the IL-6/JAK/STAT3 signalling axis in cancer. Nat Rev Clin Oncol. 2018;15:234–48.
39. Maacha S, Bhat AA, Jimenez L, Raza A, Haris M, Uddin S, et al. Extracellular vesicles-mediated intercellular communication: roles in the tumor microenvironment and anti-cancer drug resistance. Mol Cancer. 2019;18:55.
40. Hendrix MJC, Seftor EA, Hess AR, Seftor REB. Vasculogenic mimicry and tumour-cell plasticity: lessons from melanoma. Nat Rev Cancer. 2003;3:411–21.
41. Ding XS, Xi WQ, Ji J, Cai Q, Jiang JL, Shi M, et al. HGF derived from cancer-associated fibroblasts promotes vascularization in gastric cancer via PI3K/AKT and ERK1/2 signaling. Oncol Rep. 2018;40:1185–95.
42. Kim HS, Won YJ, Shim JH, Kim HJ, Kim BS, Hong HN. Role of EphA2-PI3K signaling in vasculogenic mimicry induced by cancer-associated fibroblasts in gastric cancer cells. Oncol Lett. 2019;18:3031–38.
43. Carmona-Cuenca I, Roncero C, Sancho P, Caja L, Fausto N, Fernández M, et al. Upregulation of the NADPH oxidase NOX4 by TGF-beta in hepatocytes is required for its pro-apoptotic activity. J Hepatol. 2008;49:965–76.
44. Zhang JH, Li HC, Wu QP, Chen YM, Deng YC, Yang ZC, et al. Tumoral NOX4 recruits M2 tumor-associated macrophages via ROS/PI3K signaling-dependent various cytokine production to promote NSCLC growth. Redox Biol. 2019;22:101116.

45. Ju HQ, Ying HQ, Tian T, Ling JH, Fu J, Lu Y, et al. Mutant Kras- and p16-regulated NOX4 activation overcomes metabolic checkpoints in development of pancreatic ductal adenocarcinoma. Nat Commun. 2017;8:14437.
46. Gregg JL, Turner RM, Chang GM, Joshi D, Zhan Y, Chen L, et al. NADPH oxidase NOX4 supports renal tumorigenesis by promoting the expression and nuclear accumulation of HIF2α. Cancer Res. 2014;74:3501–11.
47. Tang CT, Lin XL, Wu S, Liang Q, Yang L, Gao YJ, et al. NOX4-driven ROS formation regulates proliferation and apoptosis of gastric cancer cells through the GLI1 pathway. Cell Signal. 2018;46:52–63.
48. Lin XL, Yang L, Fu SW, Lin WF, Gao YJ, Chen HY, et al. Overexpression of NOX4 predicts poor prognosis and promotes tumor progression in human colorectal cancer. Oncotarget. 2017;8:33586–600.
49. Zhou M, Yang H, Learned RM, Tian H, Ling L. Non-cell-autonomous activation of IL-6/STAT3 signaling mediates FGF19-driven hepatocarcinogenesis. Nat Commun. 2017;8:15433.
50. Chang RX, Song LL, Xu Y, Wu YJ, Dai C, Wang XY, et al. Loss of Wwox drives metastasis in triple-negative breast cancer by JAK2/STAT3 axis. Nat Commun. 2018;9:3486.
51. Gao SP, Mark KG, Leslie K, Pao W, Motoi N, Gerald WL, et al. Mutations in the EGFR kinase domain mediate STAT3 activation via IL-6 production in human lung adenocarcinomas. J Clin Invest. 2007;117:3846–56.

Figures

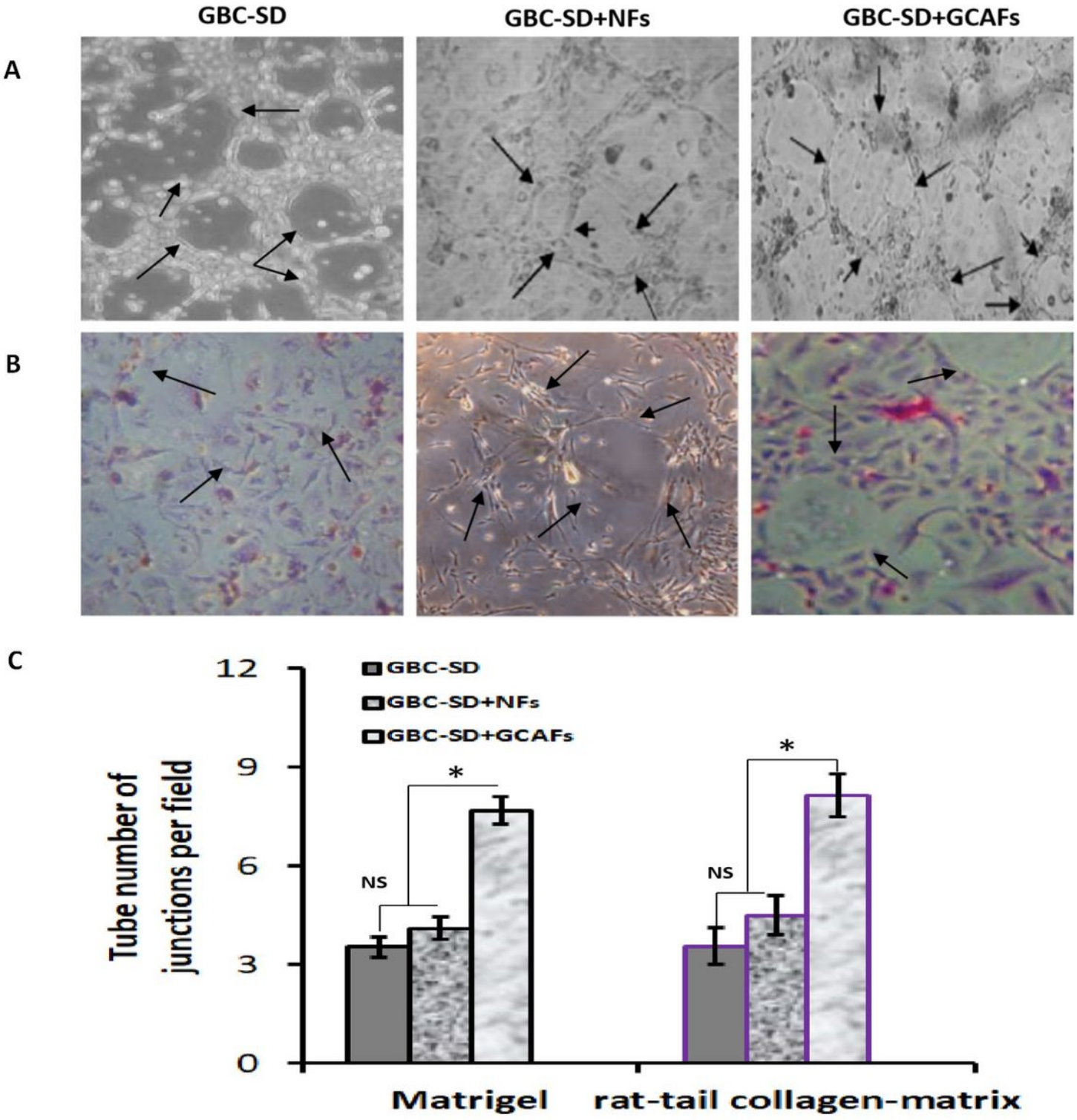

Figure 1

GCAFs promote VM formation of GBC-SD cells in vitro (Phase contrast microscopy on 3-D cultures, ×200; A: Matrigel, B: rat-tail collagen-matrix). The tube number of vasculogenic-like networks in GBC-SD+GCAFs groups was significantly more than that of GBC-SD and GBC-SD+NFs groups (all *P<0.05); furthermore, PAS positive, cherry-red materials found in granules and patches in the cytoplasm of GBC-SD cells appeared around the signal cell or cell clusters.

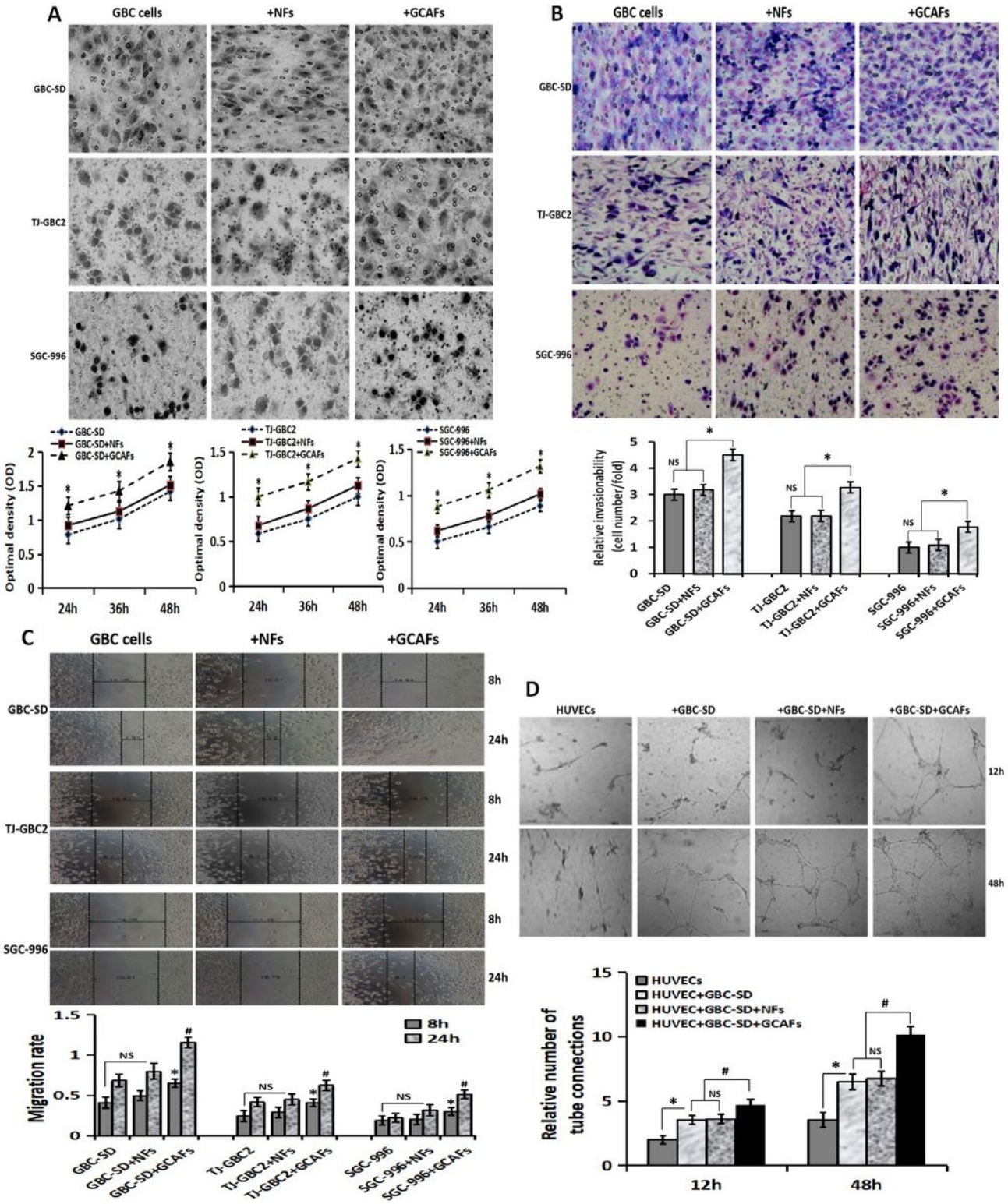

Figure 2

GCAFs promote the malignant phenotypes of GBC cells/HUVECs. (A), Proliferation assay, the proliferation ability of GBC cell+GCAFs group was significantly enhanced compared with alone GBC cell group and GBC cell+NFs group (all *P<0.05). (B), Transwell invasion assay (Giemsa stain, ×200), the number (relative invasion ability) of cells that invaded through the basement membrane in GBC cell+GCAFs group was significantly more than that of GBC cell group and GBC cell+NFs group (all *P<0.05). (C), Wound

healing assay, the cell migration rate of GBC cell+GCAFs group was significantly stronger than that of GBC cell group and GBC cell+NFs group (8h: all *P<0.05; 24h: all #P<0.05). (D), Tube formation assay, at 12h: HUVEC group (-); HUVEC+GBC-SD (+), HUVEC+GBC-SD+NFs (+), *P<0.05; HUVEC+GBC-SD+GCAFs (+), #P<0.05. At 48h: obvious tubular formation was observed in all the four groups, the number of tube formed in HUVEC+GBC-SD+GCAFs group was significantly more than that in the other three groups (#P<0.01), but no statistical difference was observed between HUVEC+GBC-SD group and HUVEC+GBC-SD+NFs group.

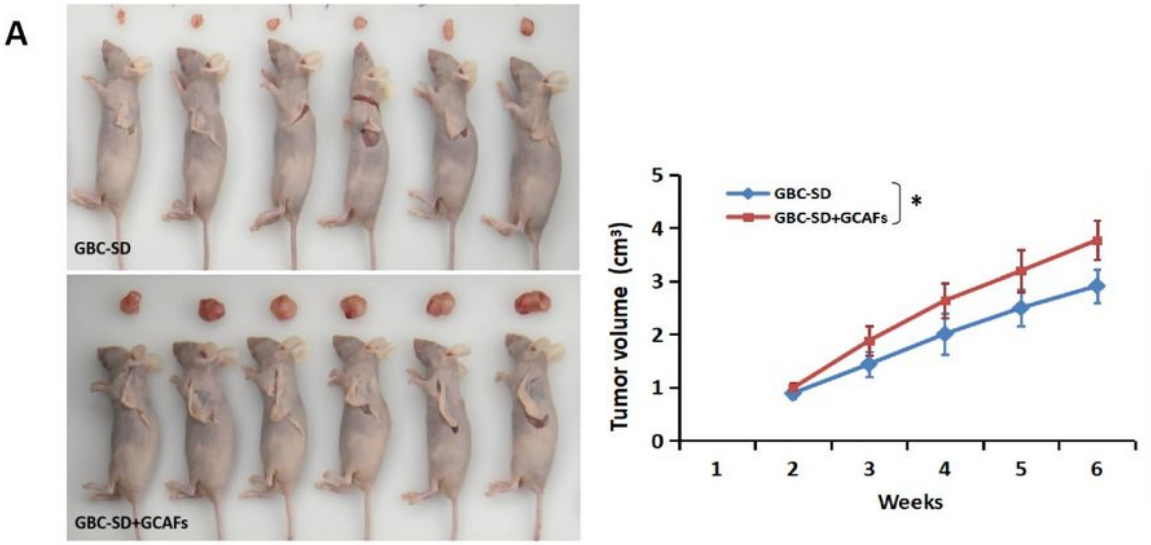

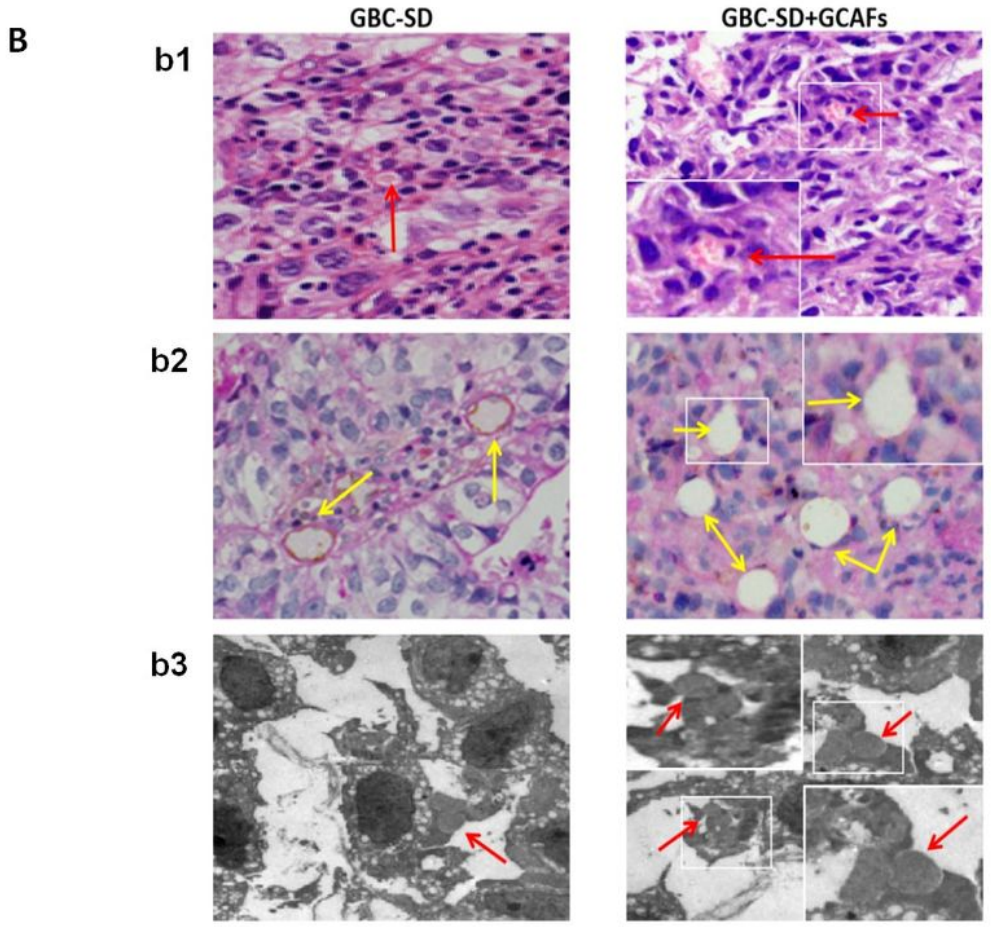

Figure 3

GCAFs promote the tumor growth and VM formation in the xenografts of nude mice. A. Size, volume and growth curves of tumor xenografts in GBC-SD+GCAFs group were significantly larger than that of GBC-SD group (*P<0.05). B (b1. HE staining, b2. CD31-PAS double stainings; ×200). Sections of the xenografts in GBC-SD group and GBC-SD+GCAFs group showed tumor cell-lined vessel-like structure with single or multiple red blood cells inside (red arrowhead) without any evidence of tumor necrosis, and PAS-positive substances line the channel-like structures (yellow arrowhead). Of them, more tumor cell-lined vessel-like structures with multiple red blood cell inside and more PAS-positive substances lining the channel-like structures of the xenograft sections in GBC-SD+GCAFs group were observed. TEM (b3; original magnification, ×8000) clearly visualized single (GBC-SD group) or multiple (GBC-SD+GCAFs group) red blood cells in the central of tumor nests in the xenografts (red arrowhead).

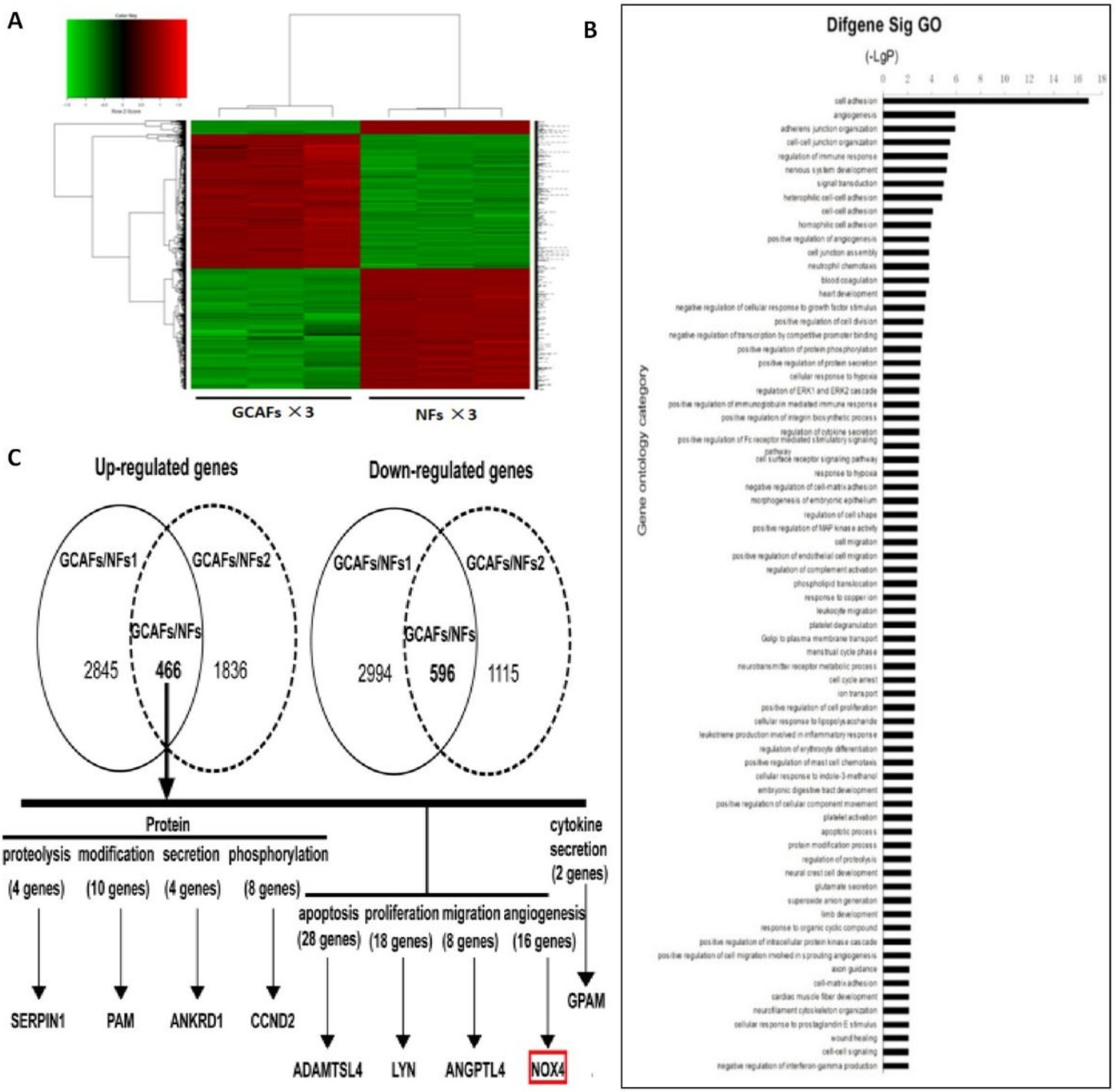

Figure 4

Identification of upregulated NOX4 expression in GCAFs in vitro. (A) Affymetrix chip analysis of gene expression profile for GCAFs and NFs using the Affymetrix GeneChip Human 1.0ST array (red color denotes upregulation and green denotes downregulation). (B) Gene ontology (GO) analysis showed upregulated expression genes, based on classification of gene numbers such as biological processes. (C) A total of 466 upregulated genes (FC>1.5) and 596 downregulated genes (FC<0.67) were identified in GCAFs/NFs according to the inclusion criteria, and NOX4 gene was significantly upregulated (FC=2.58) in GCAFs compared with NFs.

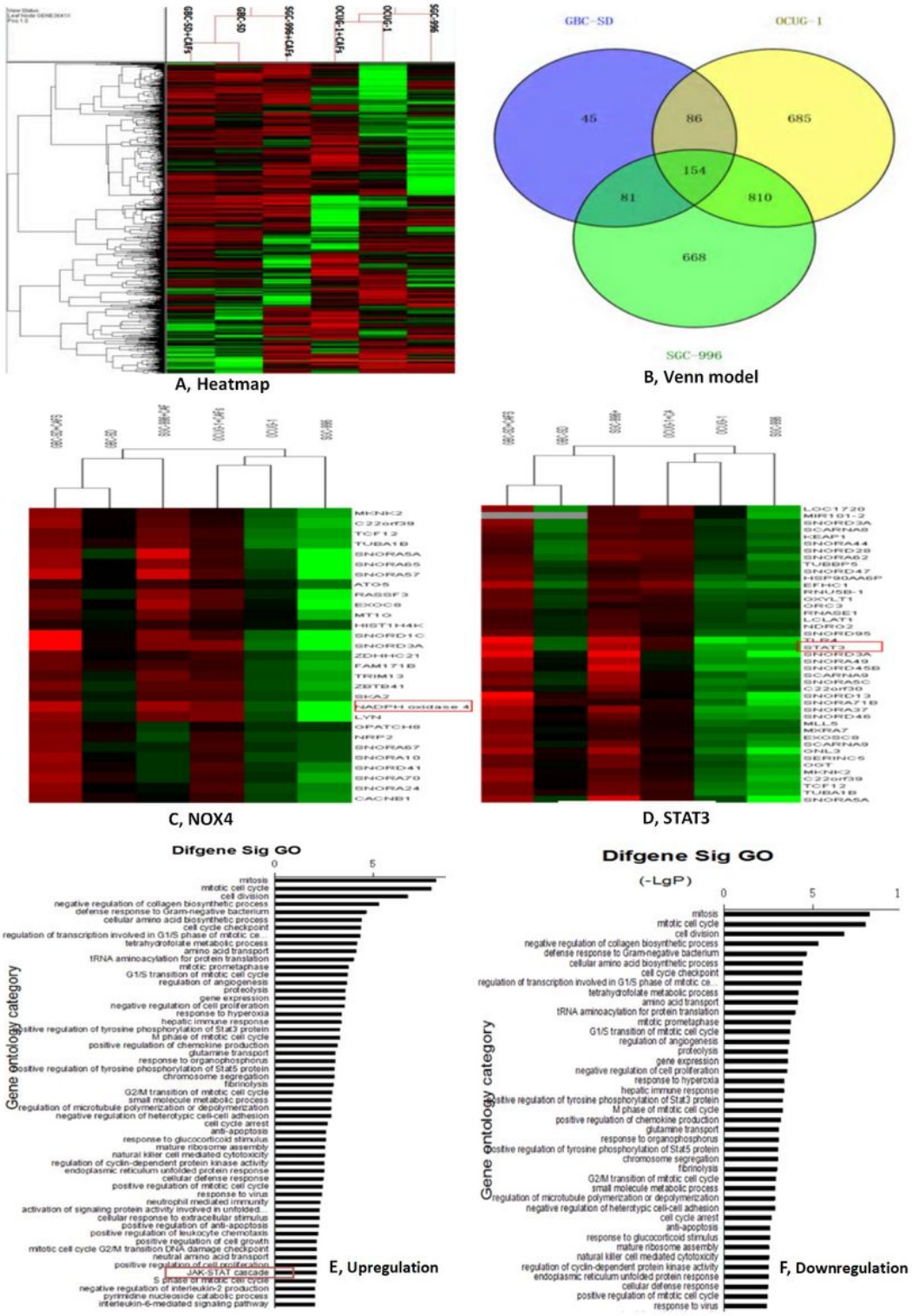

Figure 5

lncRNAs chip analysis of VM-related gene expression profile of GBC. (A), Heatmap of gene chip; (B), Venn modal analysis; (C), NOX4; (D), STAT3; (E-F), GO analysis, upregulation >2 times (E) or downregulation <0.5 times (F). Venn modal analysis of upregulation (>2 times) or downregulation (<0.5 times) genes showed JAK-STAT cascade and the high-expression of STAT3 and NOX4 in 154 of VM-related genes.

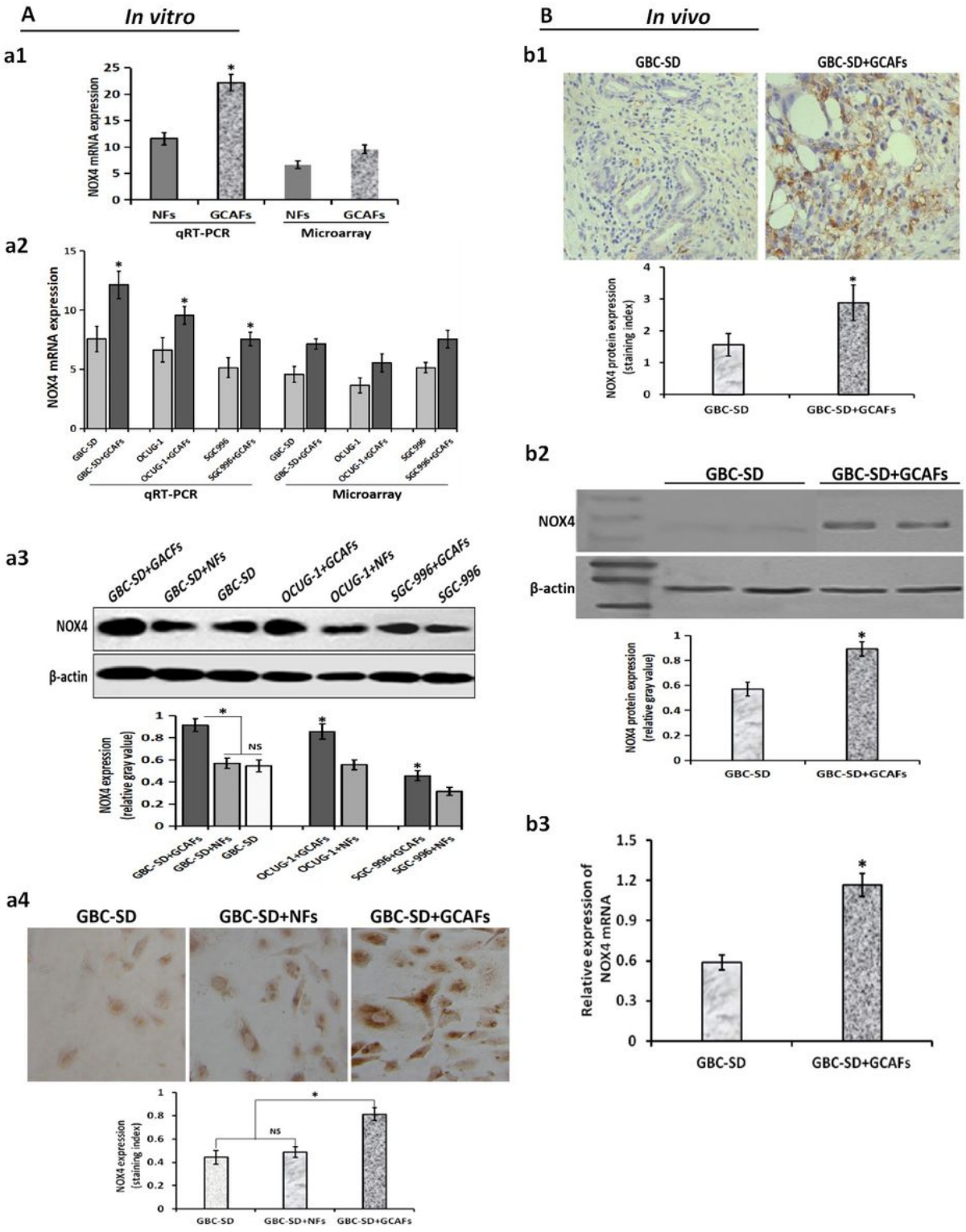

Figure 6

Verification of NOX4 expression during GCAFs-trggered VM formation in vitro and in vivo. (A), in vitro. (a1) qRT-PCR in GCAFs/NFs. NOX4 mRNA expression in GCAFs was significantly upregulated compared to NFs (*P<0.05). (a2) qRT-PCR in 3-D matrices. NOX4 mRNA expression in 3-D matrices of GBC cells (GBS-SD, SGC-996, OCUG-1)+GCAFs co-culture was significantly higher than that of alone GBC cells culture (all *P<0.05). (a3) Western blotting in 3-D matrices. The expression of NOX4 protein in 3-D

matrices of GBC cells+GCAFs co-culture was significantly upregulated compared with GBC cell+NFs co-culture and alone GBC cells culture (all *P<0.05). (a4) IHC (×200) in 3-D matrices. The expression of NOX4 protein in 3-D matrices of GBC-SD+GCAFs co-culture was significantly higher than that of GBC-SD+NFs co-culture or alone GBC-SD culture (all *P<0.05), but no statistical difference was observed between GBC-SD+NFs group and GBC-SD group. (B), in vivo. (b1), IHC (×200), (b2) western blotting. The expression of NOX4 protein in GBC-SD+GCAFs xenografts was significantly higher than that of GBC-SD xenografts in vivo (all *P<0.05). (b3), qRT-PCR. The expression NOX4 mRNA in GBC-SD+GCAFs xenografts was significantly upregulated compared with GBC-SD xenografts in vivo (*P<0.05).

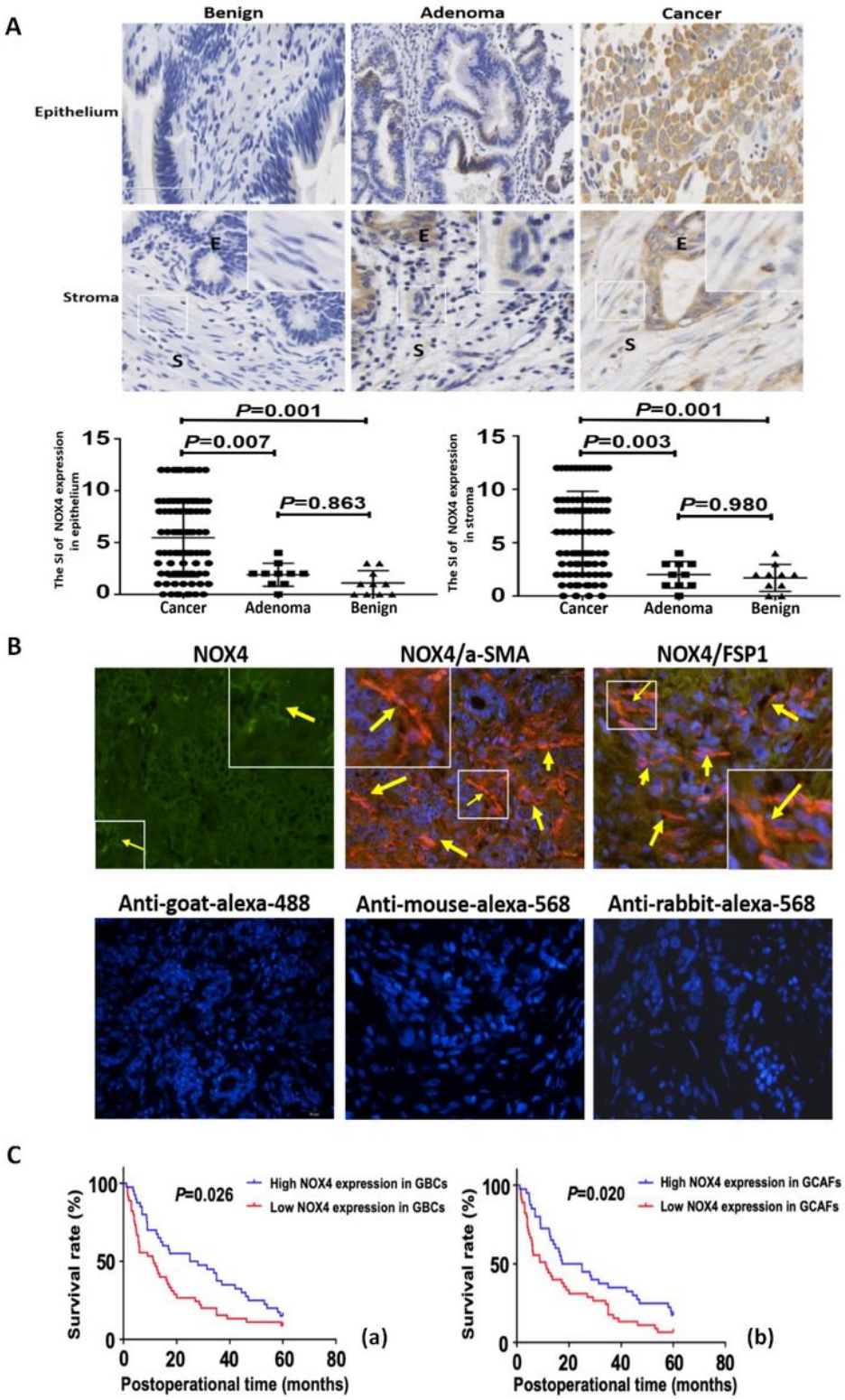

Figure 7

NOX4 is highly expressed in human GBC tissue and stroma, and is associated with poor prognosis. A (IHC, ×200; E=epithelium, S=Stroma). The expression (cytoplasmic and/or nuclear brown staining) of NOX4 in GBC cells and stroma (n=85) was significantly upregulated compared with gallbladder precancerous (adenomas, n=10; P=0.007, P=0.003) and benign lesions (cholecystitis, n=10; both P=0.001), but no statistical difference between precancerous lesions and benign lesions (both P>0.05).

Magnified insets show representative NOX4 staining in stroma. B (CIF staining, ×200). The expression of NOX4 (green) co-localizes with α-SMA and FSP1 (red) positive stroma. Representative samples of NOX4, α-SMA and FSP1 are shown. Secondary antibody only controls are shown: anti-goat-alexa-488 for NOX4, anti-mouse-alexa-568 for α-SMA and anti-rabbit-alexa-568 for FSP1. Arrows and inset point to positive staining in fibroblastic cells. C. Kaplan-Meier analysis of GBC patients with high and low NOX4 expression in GBC cells/stroma. The survival time of GBC patients with high NOX4 expression in tumor cells or stroma was significantly shorter than that of GBC patients with low NOX4 expression (log-rank test, (a), GBCs; P=0.026; (b), GCAFs, P=0.020).

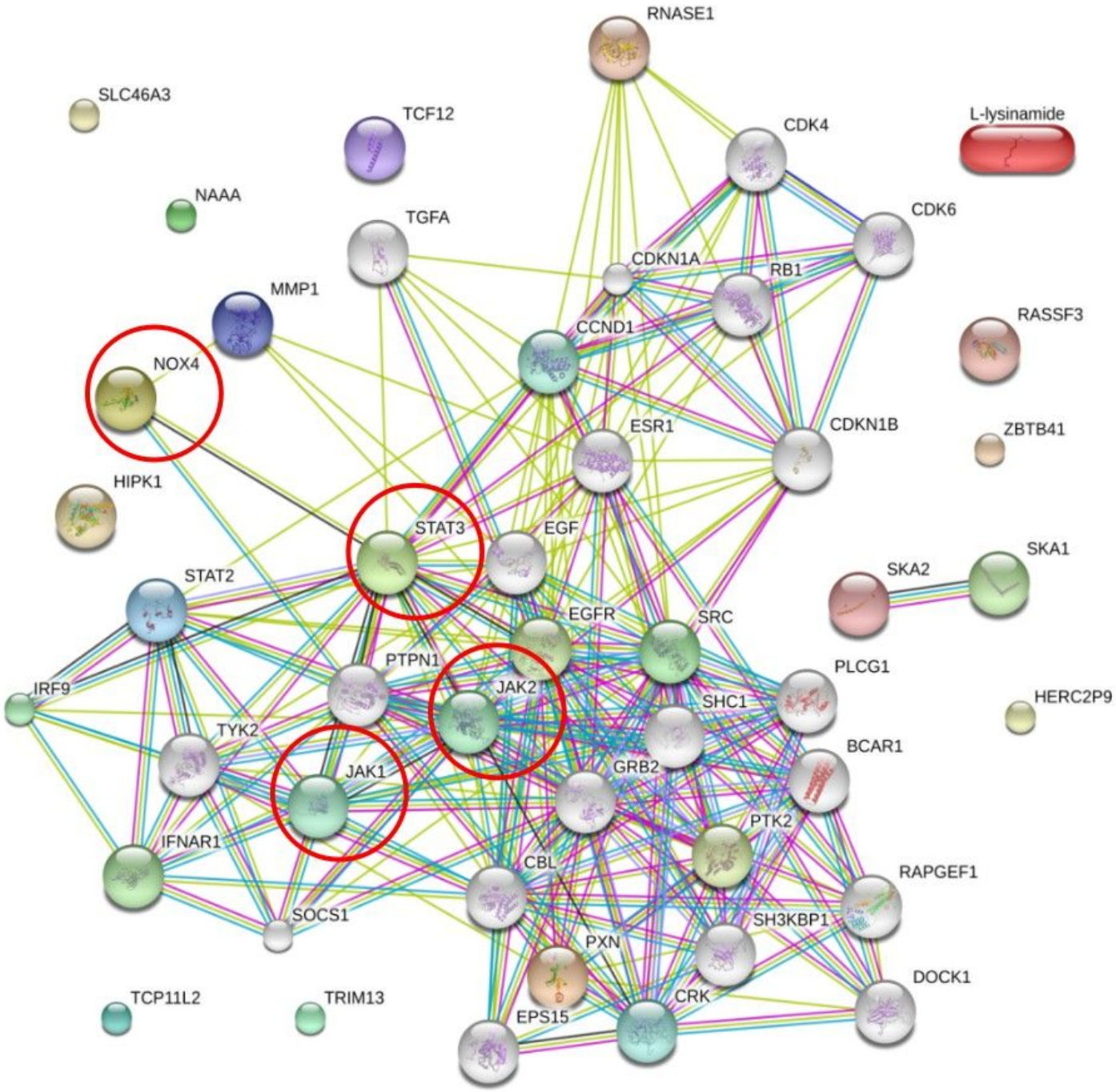

Figure 8

A network regulation model of GCAFs promoting VM formation of GBC. NOX4, STAT3, JAK1 and JAK2 are regulated in the VM-related key genes.

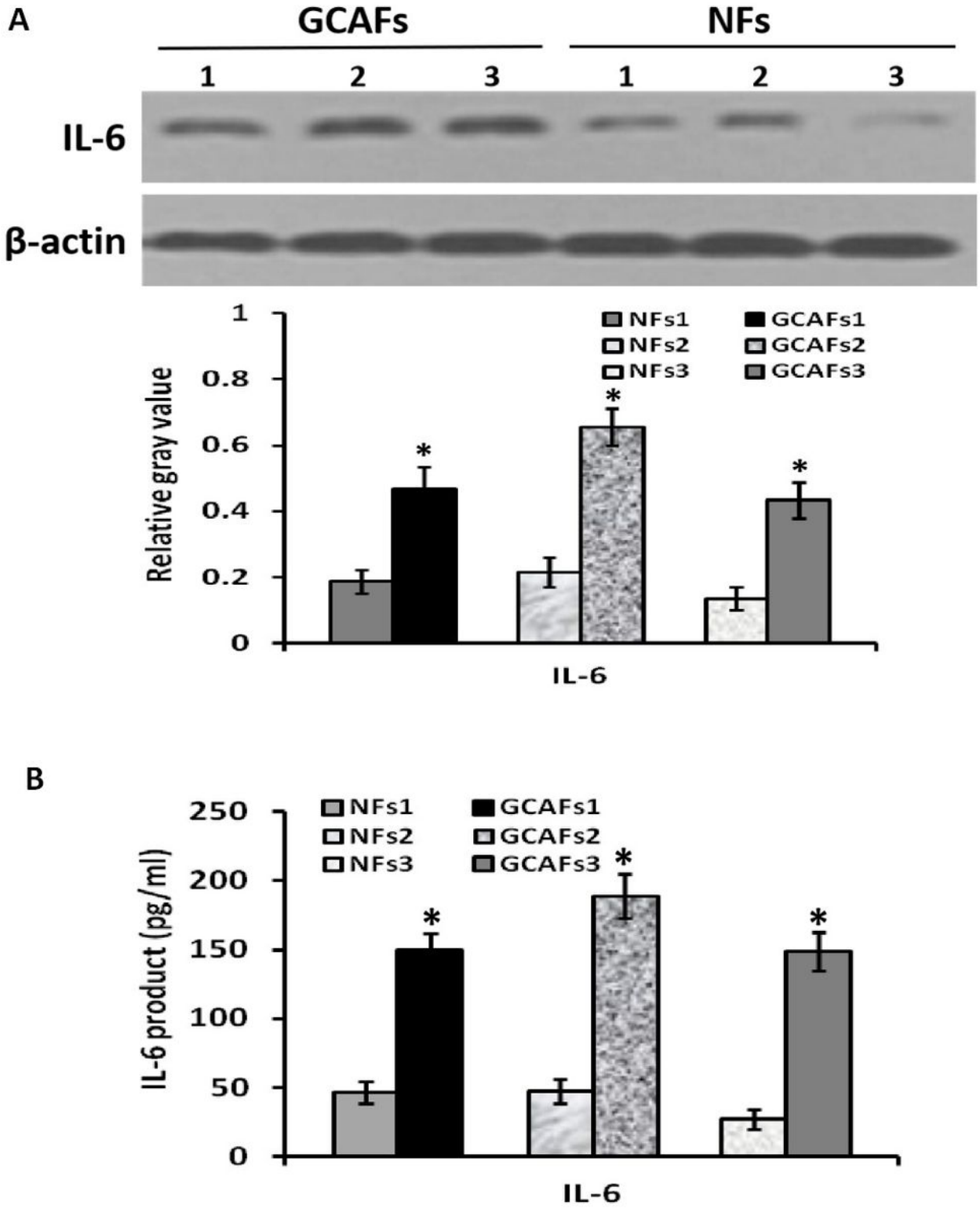

Figure 9

Confirmation of IL-6 expression in GCAFs/NFs in vitro. A (Western blotting). IL-6 protein was highly secreted and up-expressed in GCAFs compared with NFs (all *P<0.05). B (ELISA). High-secretion and up-expression of IL-6 product in the culture supernatant of GCAFs compared with NFs (all *P<0.05).

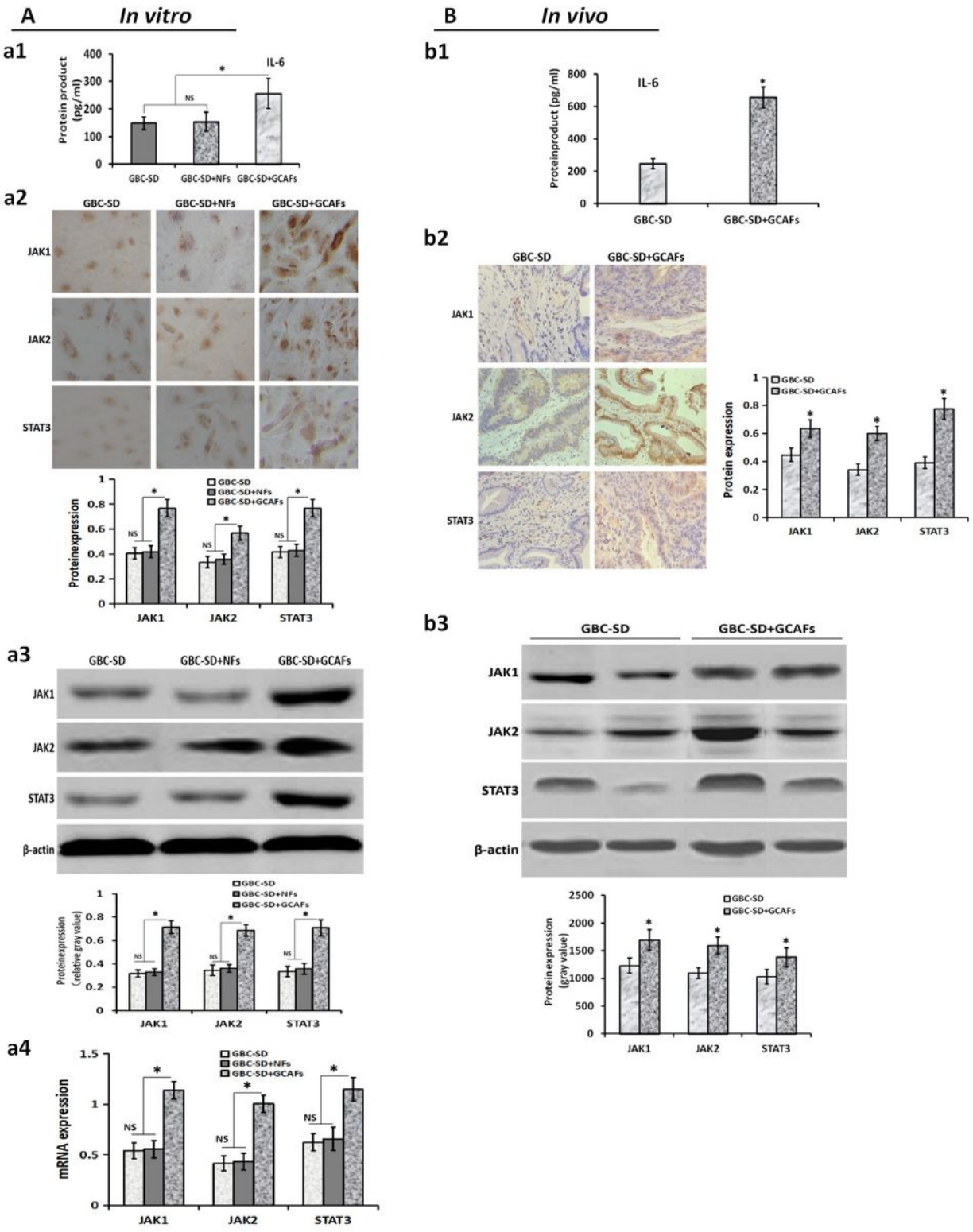

Figure 10

Verification the expression of IL-6/JAK/STAT3 signaling pathway genes in vitro and vivo. A (in vitro): a1 (ELISA), the expression of IL-6 product in the supernatant of GBC-SD+GCAFs co-culture was significantly higher than that of GBC-SD or GBC-SD+NFs co-culture (*P<0.05). a2-a3 (a2, IHC, ×200; a3, western blotting), the expression of JAK1, JAK2 and STAT3 proteins in the 3-D co-culture matrices of GBC-SD+GCAFs was significantly higher than that of GBC-SD or GBC-SD+NFs co-culture (all *P<0.05). a4 (qRT-

PCR), the expression of JAK1, JAK2 and STAT3 mRNAs in the 3-D co-culture matrices of GBC-SD+GCAFs was significantly upregulated compared with GBC-SD or GBC-SD+NFs co-culture (all *P<0.05). But, no statistical difference was observed in the expression of JAK1, JAK2 and STAT3 at protein or mRNA level between GBC-SD and GBC-SD+NFs groups. B (in vivo): b1 (ELISA), the expression of IL-6 product in the supernatant of GBC-SD+GCAFs group was significantly upregulated when compared with GBC-SD in xenografts (*P<0.05). b2-b3 (IHC, ×200; b3,Western blotting), The expression of Jak1, JAK2 and STAT3 proteins in GBC-SD + GCAFs group was significantly higher than that of GBC-SD group in xenografts (*P<0.05).